

**FACULDADE DE ENGENHARIA DA UNIVERSIDADE DO PORTO**



**FEUP**

# **Kinect Based System Applied to Breast Cancer Conservative Treatment**

**Marco Alexandre Dias Silva**

Mestrado Integrado em Engenharia Electrotécnica e de Computadores

Orientador: Jaime dos Santos Cardoso (Prof. Dr.)

Co-orientador: Helder Filipe Pinto de Oliveira (MSc.)

26 June 2012

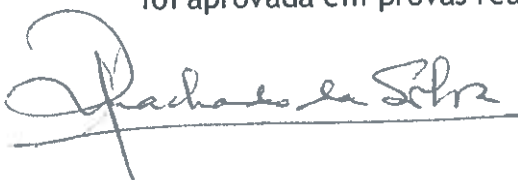


A Dissertação intitulada

“Kinect Based System Applied to Breast Cancer Conservative Treatment”

foi aprovada em provas realizadas em 25-07-2012

o júri



Presidente Professor Doutor José Alberto Peixoto Machado da Silva  
Professor Associado do Departamento de Engenharia Electrotécnica e de  
Computadores da Faculdade de Engenharia da Universidade do Porto



Professor Doutor Miguel Tavares Coimbra  
Professor Auxiliar Departamento de Ciência de Computadores da Faculdade de  
Ciências da Universidade do Porto



Professor Doutor Jaime dos Santos Cardoso  
Professor Auxiliar do Departamento de Engenharia Electrotécnica e de  
Computadores da Faculdade de Engenharia da Universidade do Porto



Mestre Helder Oliveira  
Investigador do INESC - TEC

O autor declara que a presente dissertação (ou relatório de projeto) é da sua exclusiva autoria e foi escrita sem qualquer apoio externo não explicitamente autorizado. Os resultados, ideias, parágrafos, ou outros extratos tomados de ou inspirados em trabalhos de outros autores, e demais referências bibliográficas usadas, são corretamente citados.



Autor - Marco Alexandre Dias Silva

Faculdade de Engenharia da Universidade do Porto

# Resumo

O Tratamento Conservador do Cancro da Mama é atualmente o procedimento padrão para tratar o cancro de mama. O Tratamento Conservador da Mama fornece taxas de sobrevivência semelhantes à mastectomia, sendo menos invasivo. Ele beneficia as pacientes com um melhor resultado estético, e é esperado às mulheres sujeitas a CT que vivam por mais tempo com os efeitos do tratamento. A avaliação do resultado estético fornece uma visão especial para identificar as principais variáveis que afetam o resultado. Inicialmente, a avaliação era realizada por um ou mais observadores através de inspeção visual, e portanto, as decisões era subjetivas apresentando disparidades quando se comparava diferentes avaliações entre diferentes instituições.

Para chegar a uma avaliação objectiva, o Breast Research Group do Instituto de Engenharia de Sistemas e Computadores do Porto (INESC TEC) desenvolveu o *software* Breast Cancer Conservative Treatment.cosmetic results (BCCT.core). Atualmente, o sistema usa fotografias frontais das pacientes, mas já se provou capaz de sofrer melhorias pela inclusão de informação tridimensional (3D), idealmente adquirida através de soluções de baixo custo. O dispositivo Kinect<sup>TM</sup> é capaz de produzir mapas de profundidade de uma cena, e permite detetar diferenças volumétricas produzindo resultados satisfatórios. O dispositivo reúne as características de baixo custo e de fácil utilização.

O trabalho realizado neste projeto visa contribuir com o aprimoramento dos dados adquiridos através do Kinect<sup>TM</sup>, e da definição de características 3D da forma da mama através desses dados. Contudo, as imagens apresentam uma relativa baixa resolução que pode obstruir a construção de um modelo fiel da mama. Como tal, é apresentado um estudo comparativo sobre o desempenho de algoritmos de Super-Resolução (SR), aplicados às imagens recolhidas. A obtenção de imagens de resolução superior pode tornar-se essencial para o seu posterior processamento. Além disso, é efetuada a deteção de características 3D e posterior comparação com métricas reais obtidas por um especialista. Com a inclusão de dados de mais dimensões, esperamos melhorar o desempenho do atual sistema de avaliação.

A aplicação de SR nas imagens usadas neste projeto revelou ser bem sucedida. Contudo, ao comparar os resultados obtidos na extração de características 3D face às imagens originais, não se verificou qualquer ganho adicional. Não obstante com estes resultados, a deteção de características 3D proporcionou bons resultados com uma forte correlação para as métricas reais.



# Abstract

Breast Cancer Conservative Treatment (BCCT) is nowadays the standard procedure to treat breast tumours. It provides similar survival rates then mastectomy, with a less invasive intervention. It benefits the patients with better cosmetic outcomes, and women who undergo Breast Conservative Treatment (BCT) are expected to cope with the treatment consequences for an extended period of time. The assessment of the aesthetical outcome provides insight to identify key variables that affect the outcome. Initially, the assessment was performed by one or more observers through visual inspection, and inheritably, decisions are subjective, presenting disparities when comparing different assessments from different institutions.

To reach an objective assessment, the Breast Research Group at Instituto de Engenharia de Sistemas e Computadores do Porto (INESC TEC) developed the Breast Cancer Conservative Treatment.cosmetic results (BCCT.core) software tool. Currently, the system uses frontal patient's photographs, but has proved capable of being improved by the incorporation of tri-dimensional (3D) data, ideally acquired through a low-cost solution. A Kinect<sup>TM</sup> device can render a depth-map of a scene, and allowed to detect volumetric differences with satisfactory results. This device is both low-cost and user-friendly.

This project's work aims to contribute with the enhancement of the data collected from a Kinect<sup>TM</sup> device, and the definition of 3D features of the breast shape with the data gathered from the device. Although, the relative low-resolution images captured may obstruct the construction of a reliable model. Therefore, a comparative study of the application of state-of-the-art Super-Resolution (SR) algorithms applied to captured images is presented. This may be essential before further processing in later steps. Furthermore, 3D features detection is performed and compared against real metrics performed by a physician. With the inclusion of data with more dimensionality we expect to improve the current evaluation system.

The applicability of SR onto this project's images was quiet successful. However, when comparing the results for 3D features between original with the enhanced images, we can state that no benefit was shown. Notwithstanding with these results, the detection of 3D features provided good results with strong correlation to real metrics.



# Acknowledgements

To Prof. Dr. Jaime dos Santos Cardoso for his orientation and support throughout this project.

To Hélder Filipe Pinto de Oliveira for his invaluable advisory and to be available all the time. Even at weekends.

To INESC TEC for providing me a workplace, and to all at Breast Research Group to whom I thank for their support and their talks.

To the UTM team. To Salta.

A special appreciation must be left here to those who are part of my life. Thank you. I couldn't do it without you. All of you. (minus despicable people).

To the reader, whoever you might be, I hope the conclusions drawn here are helpful to you in some way.

Marco Dias Silva





*“Prepare for unforeseen consequences.”*

G-man



# Contents

<b>1</b>	<b>Introduction</b>	<b>1</b>
1.1	Context . . . . .	1
1.2	Motivation . . . . .	1
1.3	Objectives . . . . .	2
1.4	Contributions . . . . .	2
1.5	Structure . . . . .	3
<b>2</b>	<b>Breast Cancer</b>	<b>5</b>
2.1	The Conservative Treatment . . . . .	5
2.2	Aesthetical Evaluation of Breast Interventions . . . . .	6
2.3	Motivation for Objective Evaluation . . . . .	6
<b>3</b>	<b>Objective Evaluation of BCCT</b>	<b>9</b>
3.1	3D models on BCCT . . . . .	10
3.2	Previous Developments on BCCT.core . . . . .	13
3.3	Kinect Sensor as a Tool . . . . .	16
<b>4</b>	<b>Super-Resolution Application</b>	<b>19</b>
4.1	Super-Resolution . . . . .	19
4.1.1	Super-Resolution Applied to Depth Maps . . . . .	21
4.2	Kinect Specification Assessment . . . . .	22
4.3	Performance Tests . . . . .	25
4.4	Performance Evaluation . . . . .	27
4.5	Results . . . . .	28
4.5.1	Depth Images . . . . .	28
4.5.2	Bounding Box . . . . .	29
4.5.3	RGB Images . . . . .	29
4.5.4	Synthetic Images . . . . .	31
4.5.5	Extended Set . . . . .	33
4.6	Discussion . . . . .	33
<b>5</b>	<b>Feature Detection</b>	<b>35</b>
5.1	Relevant Measures . . . . .	35
5.2	Data Acquisition . . . . .	35
5.3	Tests Results . . . . .	38
5.3.1	Volume . . . . .	38
5.3.2	Surface Area . . . . .	39
5.3.3	Breast Height . . . . .	40

5.4	Discussion . . . . .	42
<b>6</b>	<b>Conclusions and Future Work</b>	<b>45</b>
6.1	Conclusions . . . . .	45
6.2	Future Work . . . . .	46
	<b>References</b>	<b>47</b>

# List of Figures

3.1	BCCT.core interface. . . . .	9
3.2	BAT interface. . . . .	10
3.3	Application example from Farinella et al. [1] . . . . .	11
3.4	Application example from Balaniuk et al. [2] . . . . .	12
3.5	Example of divergence angles on a 3D model from Catanuto et al. [3] . . . . .	12
3.6	Example of colour based map from Catanuto et al. [3] . . . . .	13
3.7	Contour results from Cardoso et al. [4] . . . . .	14
3.8	Example of lateral view information from Oliveira et al. [5]. (a) Typical Photograph; b) Illustration showing the lines of measurement.) . . . . .	14
3.9	Kinect <sup>TM</sup> acquisition from Oliveira et al. [6]. (a) Photograph acquired with normal camera; b) Disparity map acquired with Kinect <sup>TM</sup> device.) . . . . .	15
3.10	Automatic contour detection on depth images from [7] - ground truth (solid red line), detected (dashed white line) . . . . .	16
3.11	Avatar reconstruction process. [8]. . . . .	17
3.12	Results example of mannequin from Cui and Stricker et al. [9] . . . . .	17
3.13	Surfel update demonstration in Henry et al. [10]. (a) Initial frame; b) Complete updated surfel with 95 RGB-D images. . . . .	18
4.1	Aliasing in high frequency zones in ISO 12233 chart [11]. . . . .	19
4.2	Experimental results from Yang et al. [12] . . . . .	21
4.3	Experimental results from Garro et al. [13]. (a) Input image; b) Output image. . . . .	22
4.4	Kinect <sup>TM</sup> capture setup #2. (a) RGB image; b) Depth image. . . . .	23
4.5	Depth Curve. . . . .	23
4.6	Block depth curves. (a) Frontal blocks; b) Rear blocks. . . . .	24
4.7	Block depth curves. (a) RGB Image; b) Frontal blocks; c) Middle blocks; d) Rear blocks . . . . .	25
4.8	Block depth curves with of blocks spaced 0.2 or 0.6cm. (a) Frontal blocks (0.2cm); b) Frontal blocks (0.6cm); c) Middle blocks (0.2cm); d) Middle blocks (0.6cm); e) Rear blocks (0.2); f) Real blocks (0.6). . . . .	26
4.9	Example of programs GUI. a) Program#1 GUI; b) Program#4 GUI. . . . .	28
4.10	Example of Bounding Box SR on image 074. (a) Original; b) Output of program#8; c) Output of program#10; d) Output of program#11. . . . .	30
4.11	Example of application of SR in RGB images (a) Original; b) output of program#1; c) Output of program#5; d) Output of program#10. . . . .	31
4.12	Example of application of SR in synthetic images (a) Original; b) output of program#1; c) Output of program#5; d) Output of program#10. . . . .	32
5.1	3D plot of breast surface (backwards view). . . . .	36

5.2	Illustration of rotation estimation points. . . . .	37
5.3	Illustration of computable area for plane definition. . . . .	37
5.4	Medical expert performing measures. . . . .	37
5.5	Scatter plot of volume ratios. a) Without rotation compensation; b) With rotation compensation. . . . .	39
5.6	Scatter plot of area ratios. a) Without rotation compensation; b) With rotation compensation. . . . .	40
5.7	Scatter plot of depth height ratios. a) Without rotation compensation; b) With rotation compensation. . . . .	41
5.8	Scatter plot of estimated metric height ratios. a) Without rotation compensation; b) With rotation compensation. . . . .	42
5.9	Scatter plot of height ratios (no rotation compensation). a) From program#5 output; b) From program#8 output. . . . .	43
5.10	Scatter plot of height ratios after rotation compensation. a) From program#5 output; b) From program#8 output. . . . .	44

# List of Tables

4.1	Tested Programs . . . . .	27
4.2	Performance Trial . . . . .	29
4.3	Bounding Box Performance Overview . . . . .	29
4.4	RGB Performance Overview . . . . .	30
4.5	Synthetic Image Performance Overview . . . . .	33
4.6	Performance Overview . . . . .	33
5.1	Volume Data Without Rotation Compensation . . . . .	39
5.2	Volume Data With Rotation Compensation . . . . .	39
5.3	Area Data Without Rotation Compensation . . . . .	40
5.4	Area Data With Rotation Compensation . . . . .	40
5.5	Depth Height Data Without Rotation Compensation . . . . .	41
5.6	Depth Height Data With Rotation Compensation . . . . .	41
5.7	Estimated Height Data Without Rotation Compensation . . . . .	42
5.8	Estimated Height Data With Rotation Compensation . . . . .	42
5.9	Correlation of height ratios between LR and HR images. . . . .	43





# Abbreviations

2D	Two-dimensional
3D	Tri-dimensional
BAT	Breast Analyzing Tool
BC	Breast Cancer
BCT	Breast Conservative Treatment
BCCT	Breast Cancer Conservative Treatment
BCCT.core	Breast Cancer Conservative Treatment.cosmetic results
BRA	Breast Retraction Assessment
BSA 0.1	Breast Shape Analyzer 0.1
cm	Centimetre
dB	Decibels
FEUP	Faculdade de Engenharia da Universidade do Porto
FoV	Field-of-View
GUI	Graphical User Interface
HR	High-resolution
IBP	Iterative Back Projection
INESC TEC	Instituto de Sistemas e de Computadores do Porto, Tecnologia e Ciência
LR	Low-resolution
MAP	Maximum a Posteriori
PGM	Portable GrayMap Format
POCS	Projection Onto Convex Sets
PSNR	Peak Signal to Noise Ration
QoL	Quality-of-Life
RBF	Radial Basis Function
RGB	Red-Green-Blue
RMS	Root Mean Square
SR	Super-Resolution
SVM	Support Vector Machine
VCMI	Visual Computing and Machine Intelligence group



# Chapter 1

## Introduction

This project intends to study applicable improvements to the Breast Cancer Conservative Treatment.cosmetic results (BCCT.core) software tool developed by the Breast Research Group<sup>1</sup> at the Instituto de Engenharia de Sistemas e Computadores do Porto (INESC TEC). It ran under the master's dissertation of the Integrated Master in Electrical and Computers Engineering at Faculdade de Engenharia da Universidade do Porto (FEUP) under the supervision of Professor Jaime dos Santos Cardoso and MSc. Hélder Filipe Pinto de Oliveira.

### 1.1 Context

Breast Cancer Conservative Treatment (BCCT) is nowadays the standard procedure to treat breast tumours. Initially, the assessment of the aesthetical outcome was performed by visual inspection by one or more observers. Inheritably, decisions were subjective and presented disparities when comparing different assessments. Therefore, the inexistence of general measurements for the cosmetic outcome led the necessity of replacing the subjective evaluation with an objective and reproducible method.

The Breast Research Group group developed the BCCT.core to suppress this need, providing an objective evaluation of the cosmetic result. Currently it uses frontal digital images from patients, but has proved capable of being improved with the inclusion of more measurements. Through the addition of more dimensions to the captured measurements, it is possible to create a more reliable model of the shape of the breast.

Chapter 2 and 3 show an in-depth contextualization on breast cancer and its assessment, as well as current and past developments on the BCCT.core system.

### 1.2 Motivation

The usage of 3D data into such evaluation system poses many advantages but also present many challenges. The high cost of 3D equipment and the strict conditions of operation and manipulation

---

<sup>1</sup><http://medicalresearch.inescporto.pt/breastresearch/>

make it nearly impossible for the everyday use of such solution. Oliveira et al. [14] conducted a study and development of low-cost and ease of operation solutions to gather a 3D model of a female torso. The eventual conclusion was that a Kinect<sup>TM</sup> device is able to detect volumetric differences and produced satisfactory results.

With the gathered 3D data, it is possible to produce models that can be viewed from different angles, and produce more measurements that were inaccessible from patient's photographs. This represented great potential, but the acquisition system is limited to its capture resolution. The disparity maps obtained with the device have relatively low-resolution (LR) and may be a limitation to produce a clear model.

### 1.3 Objectives

Following the tendency of recent contributions to BCCT.core, the aim of this project is to contribute with enrichment of the data collected from the Kinect<sup>TM</sup> and use it to come to new 3D features definition. This will render possible to pursuit the objective of creating a fully autonomous tool and to allow further contributions in the future.

At the first stage it is needed to enhance the resolution of the images acquired with the Kinect<sup>TM</sup> device, employing SR techniques. This will allow for a more efficient 3D reconstruction of the breast shape model. Further developments will focus on the identification and acquisition of 3D features such as volume, surface area, breasts height, among others.

With these contributions and by the use of two-dimensional (2D) plus 3D information, we expect to improve, not only the performance of the current evaluation, but also its quality and consistency. Finally, it is important to compare these contributions to the standard subjective evaluation performed by medical experts, as well as to current objective methods.

### 1.4 Contributions

The work to be developed represents the starting point in the processing of 3D data from the Kinect<sup>TM</sup> device for the use in BCCT.core. It intends to:

- obtain enhanced images based on those captured from Kinect<sup>TM</sup>;
- detect 3D features;
- define new measurements;
- comprove the 3D data relevance.

The development of this work has produced a paper submitted to the StudECE 2012<sup>2</sup>, 1<sup>st</sup> PhD. Students Conference in Electrical and Computer Engineering, with the title Super-Resolution on Depth-Maps Images.

---

<sup>2</sup>[//www.fe.up.pt/ StudECE2012/](http://www.fe.up.pt/StudECE2012/)

## 1.5 Structure

This document has 6 Chapters and is structured as follow: Chapter 2 and 3 give a more in-depth contextualization on Breast Cancer and previous developments, respectively, carried by the VCMi group. Chapter 4 describes a brief overview of state-of-the-art algorithms on SR techniques and presents the discussion alongside the results of the application of SR methods on the database of images. Chapter 5 explores the 3D feature definition on the captured images and its results related to physician measurements. Both Chapter 4 and 5 are finalized by a brief summary of its contents and conclusions. Chapter 6 is the last chapter and summarizes the results and conclusions drawn to take into future developments.



## **Chapter 2**

# **Breast Cancer**

The appearance of a malign tumour that originates in the breast is called Breast Cancer (BC). From there, the tumour may spread to other areas of the body often using the lymphatic system. This type of cancer is fairly common and potentially lethal. Although any person can develop BC, it is currently most found in women. Also, it is the most common type of cancer that strikes the gender [15].

The procedures for local treatment of BC can roughly be considered as surgical treatments, but chemo or radiation therapy is also employed in conjunction with surgery. Most surgery techniques are lumpectomy or mastectomy based, although quadrantectomy may also occur. In lumpectomy, only the cancerous cells are extracted while trying to preserve the most surrounding tissue as possible. While in the mastectomy, it is performed the removal of the entire breast. Variations of this procedure that do not accomplish the total removal of the breast are preferred then a complete, radical, mastectomy [16]. Since women see the breast as part of their femininity, its removal would cause devastating effects on their self-image, and cause emotional and psychological changes [17]. Therefore, in these variations it is minimized the removal of surrounding tissue as possible, some even being approximate to lumpectomy surgeries. Posterior to these interventions, reconstruction of the breast often takes place. This has become more and more common and part of the treatment of BC.

### **2.1 The Conservative Treatment**

Aside from its high incidence rate the statistics show that 69% of the women that are diagnosed with the disease are still alive after 5 years [16]. This factor presents a clear sign that prevention and treatment techniques are crucial for the high rate survival.

Treatment techniques have also evolved to a more sustainable image of the breast, and more women are deciding to treat their breast cancers without permanent loss of the breast. The conservative approaches result in the combination of the removal of cancerous tissue by surgery with posterior complementary therapy. Posterior therapies are accomplished by radiotherapy or by



medication such as chemotherapy or hormonal therapy. These post operative therapies are essential for the complete eradication of the tumour or to reduce incidence or recurrence [16], [18]. Also, reconstructive procedures of affected areas may take place alongside or after the cancer-removing surgery.

BCCT has shown similar survival rates on patients comparing to other treatments [16], but providing better aesthetical outcomes. A good aesthetical outcome improves patient's Quality-of-Life (QoL) since they usually cope with the results for an extended period of time. The cosmetic result depends on several factors from diagnosis to tumour characteristics, patients response to treatment, and the techniques applied in the treatment [19]. The combination of these factors contributes to the diverse outcomes of cosmetic results, further facilitating the disparities in its assessment.

## 2.2 Aesthetical Evaluation of Breast Interventions

The diversity of cosmetic results on breast interventions is inhibitory of a proper classification on the procedures performance. This classification would bring knowledge of the key variables that would cause an improvement over surgical techniques and standard protocols, that are expected to have higher influence over the cosmetic result [20]. Such documentation would serve as guidelines to surgical procedures and guarantee quality assessments [19].

Traditionally, the assessment of the cosmetic result is performed by one or more observers through visual inspection of the patients or their representative photographs [21]. Inheritably, human decisions are subjective due to complex factors and any final evaluation decision is, therefore, also subjective. Usually the evaluators grade the aesthetical result by comparing measurements between the treated and non-treated breast, using one of several scales found in the literature. The most common evaluation scale was introduced by Harris in 1979 [21] and is based on a classification of the cosmetic result in four classes: excellent, good, fair, and poor. The use of different evaluation scales and the fact that some clinicians who take part in the procedure are also evaluators, make the aesthetical result interpretation rather vague. It is then, difficult to compare assessments made from different panels of observers since their level of agreement is usually low or moderate, comprising a low reproducibility in results [22].

## 2.3 Motivation for Objective Evaluation

By disparities in cosmetic assessment due to lack of standard methods, clinicians faced adversities in development or refinement of procedures to globally improve aesthetical results since some could weight key variables differently. To overcome poor reproducibility of cosmetic assessment some objective methods were introduced, consisting in measurements of identifiable points from patients photographs [23], [24]. Other groups have complemented or correlated asymmetry measurements with a sum of individual scores of subjective and objective indices [22], [25]. In 1985, Pezner et al. [26], proposed the first objective assessment measurement: the Breast Retraction

Assessment (BRA), to measure the retraction of the treated breast regarding the non-treated one. Further measurements [27] were proposed based on breast asymmetry, but most were the result of combination with subjective assessments from observers. Therefore, the lack of standardized evaluation of cosmetic outcomes continued to persist. To overcome that subjective barrier, there is a need to reach an assessment that is objective and reproducible so clinicians can use and validate others assessments.



## Chapter 3

# Objective Evaluation of BCCT

Identifying the need for an objective assessment of the cosmetic results on breast interventions, the BRG developed the software entitled BCCT.core (Fig. 3.1) [28], introducing a valuable objective tool for the BCCT aesthetic evaluation result.

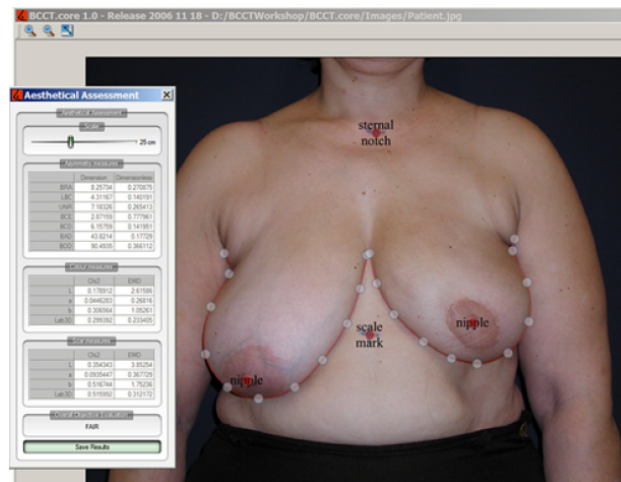


Figure 3.1: BCCT.core interface.

This software is a semi-automated tool for the assessment of the aesthetic result based on the comparison between the treated and non-treated breasts in frontal digital images from patients subjected to BCCT, producing an objectively and reproducible result. The system is capable to extract features from the patient's photographs such as: breast asymmetry, skin colour change and scar visibility [29]. To achieve this, the user must manually identify breast endpoints, nipple position and sterna notch position. Afterwards, it is capable of detecting breast contours and to automatically extract features related to the aesthetical outcome. The output of the evaluation is categorized according to Harris scale (excellent, good, fair and poor). The final objective evaluation is a summary of the overall aesthetic result, based on a Machine Learning algorithm [30], allowing the identification of which key factors influence the outcome of the treatment. It is, then,

possible to use this system as a mean to improve current treatment techniques and to compare assessments of different work teams.

Breast Analyzing Tool (BAT) [31] is another software tool that is designed to objectively assess the cosmetic outcome of breast interventions. Much like the BCCT.core, BAT uses frontal photographs of patients, but is limited to measures of asymmetry between breasts. Cardoso et al. [32] conducted a comparative study between both tools. They found that the BCCT.core scores higher consensus within medical experts evaluation, although both tools only shared moderate overall consensus. Also, the BAT tool showed performance consistency within different sets of images, to the belief of the authors, related to the picture quality. The existence of such tools like BCCT.core and BAT, give a powerful aid to clinical institutions. The possibilities of a clear evaluation and identification of key impact areas, with the capability to exchange information, opens a road for further improvements in surgical techniques.

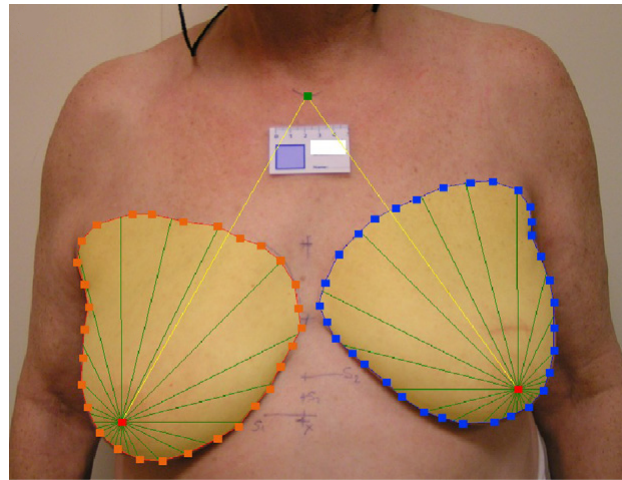


Figure 3.2: BAT interface.

Other methods have been proposed to objectively evaluate cosmetic outcomes. Lee et al [33] proposed a method that uses a curve fitting catenary to extract useful information of the breast contours using a mathematical predictive model. To the authors belief, it differentiate from simpler measurements and may allow simulation to predict likely changes to breast shapes. Kim et al. [34] developed objective measurements to evaluate the degree of breast ptosis from lateral and oblique views photographs. The presented results show higher intra- and inter-observer variability than subjective methods at fiducial points marking.

### 3.1 3D models on BCCT

Some research groups have made attempts to use 3D technology to capture the volumetric information and surface modelling [35], [36], [37], whilst more interesting approaches have been performed by Losken et al. [38], [39], [40] and Catanuto et al. [1], [3], [41], [42]. Losken et al. used a 3D camera to quantify the cosmetic result of BCCT by an objective technique. With

their system, they compare the treated and non-treated breast by analysing the surface and volume differences. Through a software program, they later analyse the level of asymmetry between the breasts using a root mean square (RMS) calculation, by mirroring on side of the patient and super-impose it with the original image. On the other hand, Farinella et al. [1] used a 3D laser scanner making use of anatomical landmarks identified by surgeons to develop the Breast Shape Analyzer 0.1 (BSA 0.1) software. By using limited well-defined anatomical endpoints, identified and selected by surgeons, the software provides an objective and quantitative measurements (Fig. 3.3).

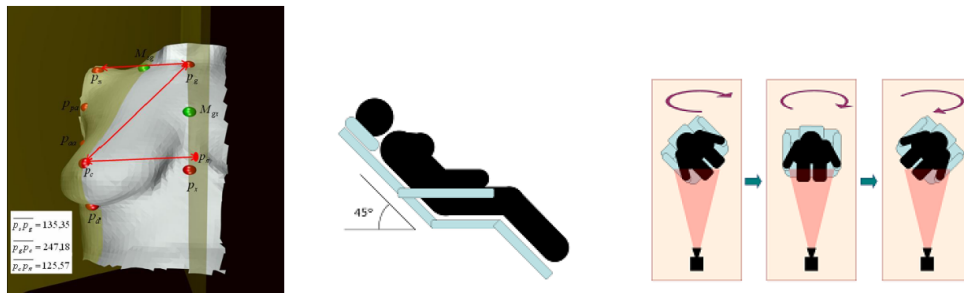


Figure 3.3: Application example from Farinella et al. [1]

The technique employed divides the breast in 4 anatomic sub-units to extract several measures that can be extrapolated onto a 3D model data set. The data was collected with a commercial laser scanner, from volunteers scanned in three different occasions, while sited on a chair with their backs tilted 45 degrees and rotating them to the left and right. The main drawback of this approach is patients' uncontrollable physiological movements, which posed a problem when merging scans.

By registering the volumetric differences through radiotherapy, Bert et al. [43], produced daily surface models. The described system registers the transformations based on the collected data and determines the rigid-body transformation.

Isogai et al. [35] developed a 3D imaging system using laser light scanning to perform a quantitative analysis. By mirroring the non-treated breast onto the reconstructed breast, the system gives an evaluation based on breast symmetry, volume and shape.

Balaniuk et al. [2] also developed a 3D imaging tool to simulate the cosmetic outcome. The system uses virtual reality combined with soft tissue modelling methods, and the authors emphasise the importance of the tool for both patients and surgeons that through simulation can make more informed decisions (Fig. 3.4).

Catanuto et al. [3], suggest a set of parameters to characterise the breast shape, such as surface, distance and angles measurements; curvature properties and symmetry analysis. Employing the same acquisition method and system to evaluate these set of parameters, the authors express that the angle calculations and the graphic depiction of the breast "curvature" are the most interesting and innovating results. The former, the "divergence angle", gives a perspective on the point of view of the patient's own breasts (Fig. 3.5); and the later introduces a representation on the breast based on a colour map to express flat regions and curvature (Fig. 3.6). The authors conclude that

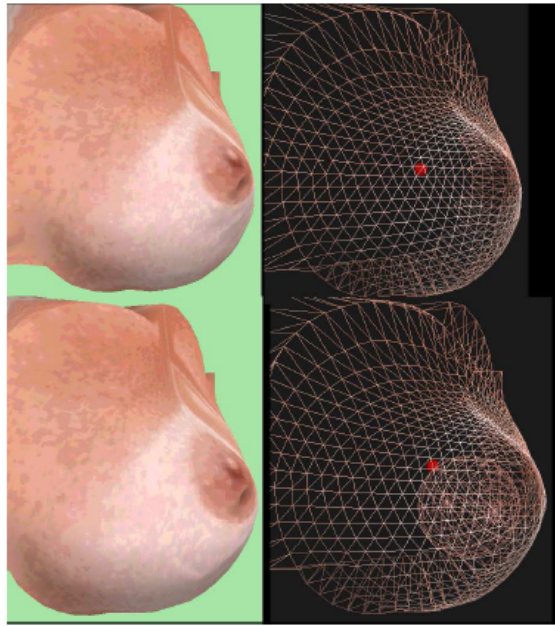


Figure 3.4: Application example from Balaniuk et al. [2]

the colour based curvature representation can replace volume terminology, as curvature can be expressed either with colours and its degree by coefficients.

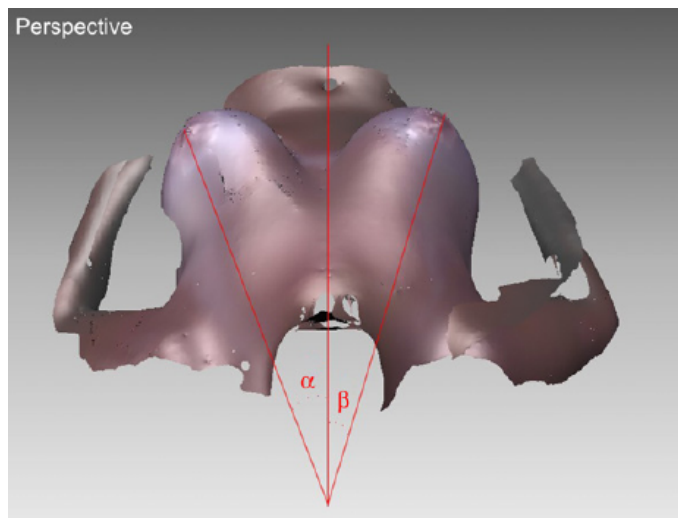


Figure 3.5: Example of divergence angles on a 3D model from Catanuto et al. [3]

Moreover, Catanuto et al. [41] present estimation and reconstruction of the breasts using an optoelectronic tracking system, which allows real-time breathing artefact correction [42] and surface patch (fusion). By applying their technique they obtain a graphic depiction of the curvature of the thoracic surface. Although interesting results come from these techniques they all show a deficit in using specialized hardware, software and personnel.

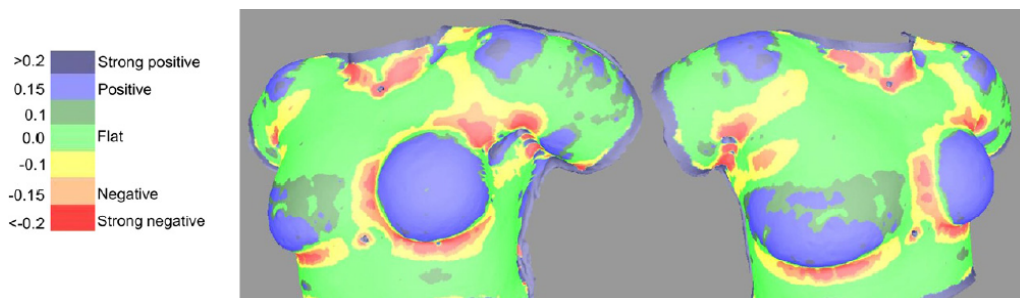


Figure 3.6: Example of colour based map from Catanuto et al. [3]

Furthermore, the use of 3D models can improve medical practice, such as surgical techniques and skills, as the software can be improved to have embedded simulation. Surgeons can boost their performance and techniques onto breast intervention procedures and also provide anticipation of surgical options and outcomes. Tepper et al. [37] provide, in their work, an overview of 3D breast photography and how they pose a potential establishment of a standardised system for breast analysis. They introduce a new concept “mammometrics”, 3D based breast measurements that can be used to guide operative planning and analyse surgical results objectively. This will help patients to build a better understanding and informed choice of surgical outcomes. Such feature’s gains increases the relevance of using 3D information in evaluating aesthetic results. Although the advantages of using a 3D model are immense its acquisition must be practical (performed by the clinicians themselves), and without using expensive equipment or requiring specialized personnel. Also the acquisition step should be fully autonomous or require minimal input from the user. Therefore, the need of simple and low cost solution that could be fit as a computer peripheral to complement the software system.

## 3.2 Previous Developments on BCCT.core

Software tools like BCCT.core and BAT for objective evaluation of the cosmetic result have proved to be viable solutions towards a standard objective evaluation [32]. In fact, BCCT.core system is already being used in several institutions. Nonetheless, these tools have still great potential for improvements. Namely on BCCT.core, there have been developments to improve its consistency and performance. At the present moment BCCT.core only uses frontal images of patients and is not totally automatic. This means that limited information is available on the breast shape, and final aesthetic evaluation result slightly depend on user inputs. In order to introduce more available information on breast shape and reach a more autonomous software tool, the VCMi group has made essays to enrich the system’s evaluation.

In [4] (Fig. 3.7) is presented an automatic breast contour detection algorithm that came to improve previous work [44]. Also, by incorporating prior shape information to the detection algorithm [45] it was verified an enhancement on the automatic detection .



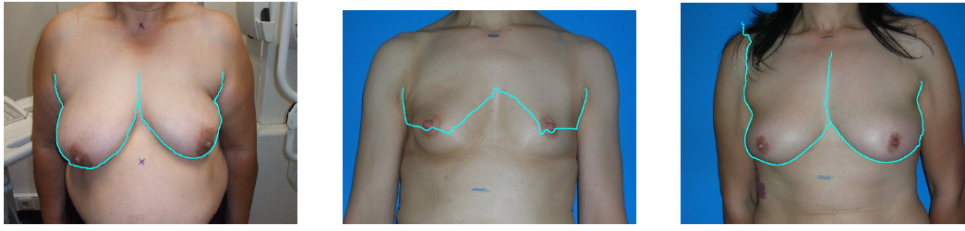


Figure 3.7: Contour results from Cardoso et al. [4]

Furthermore, in [46] proposed a method to automatically find external endpoints through the formulation of the breast contours. An often suggested improvement to BCCT.core was the interpretability of the model on which the system uses to predict overall cosmetic result. This was due to the need to understand how the model operates and the limited knowledge that clinicians have from relation between final result and feature inputs. In [47], the authors consider a linear Support Vector Machine (SVM) and Decision Trees to substitute the SVM classifier with a Radial Basis Function (RBF) fitted in BCCT.core at the time. Linear models for classification divide the input space into decision regions which are linear to the determined input, so the decision space is a simple weighted sum of input features. Therefore is simple to give higher weights to features with more relevant impact in the decision process. The authors conclude that the use of a linear model onto BCCT.core will increase its interpretability and provide validation and trust on the use of the system. In order to verify whether the lateral measures represented an increase of valuable information to improve overall assessment, the work presented in [5] provided the introduction of lateral information from patient's side-view (Fig. 3.8). From its study the authors concluded that improvements were not significant, although, it is added that the use of more robust models or 3D models would help to achieve better performance in overall cosmetic assessment.

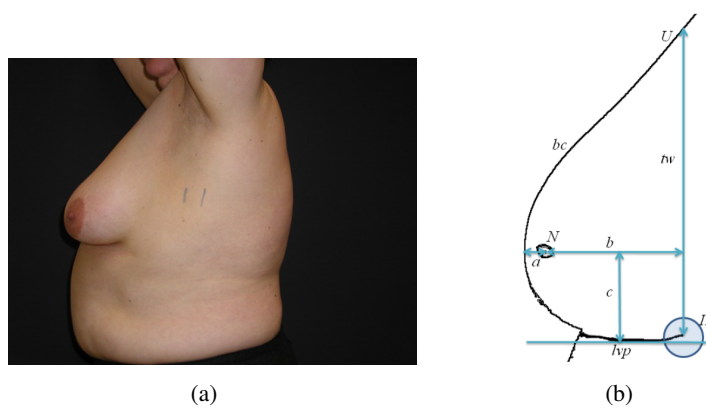


Figure 3.8: Example of lateral view information from Oliveira et al. [5]. (a) Typical Photograph; b) Illustration showing the lines of measurement.)

BCCT.core software tool has proven that is capable of being improved by providing more measures or to add dimensionality to the ones made. However female breast is a 3D shape structure

and its boundaries and volume are difficult to attain. 3D data can improve feature acquisition by producing more measurements thus optimizing the automation of the system and the final evaluation of the aesthetical result.

To the contribution of developments on BCCT.core, Oliveira et al. [14] conducted a study and development of low-cost and ease of operation solutions to gather a 3D model of a female torso. They first implemented a reconstruction algorithm from two uncalibrated views through epipolar geometry gathering acceptable results. The second implementation using a disparity map acquired by a Kinect<sup>TM</sup> device provided very satisfactory results, mainly the tests with real patients. The device allowed to detect volumetric differences, and the results were very similar to reference measures manually performed by the physician. On the 3D model reconstruction from two uncalibrated views, Soares [48] came to conclude that state-of-the-art algorithms for stereo matching failed to provide a proper reconstruction. The unsuccessful results were given to the high ambiguity that is found on the images that the project works on, and to lack of poor confident matching in image areas. It is concluded that further search or development is needed to suit the project's needs.

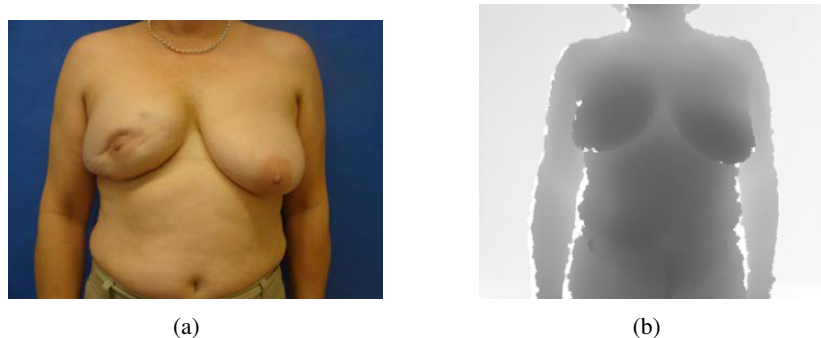


Figure 3.9: Kinect<sup>TM</sup> acquisition from Oliveira et al. [6]. (a) Photograph acquired with normal camera; b) Disparity map acquired with Kinect<sup>TM</sup> device.)

As verified in [14], [6], with the use of the Kinect<sup>TM</sup> motion sensor device is possible to generate a disparity map to use in a future 3D mesh construction. Besides, with the use of disparity maps the breast contour detection is performed without user input, so the system's automation is improved [7]. Also, the device comprises the requirements of being both low-cost and user-friendly. With the gathered 3D data is possible to produce models that can be viewed from different angles and produce more measurements based on that data that is inaccessible from patient's photographs, alone or combined. This would bring BCCT.core valuable measurements to complement its overall aesthetical assessment of breast interventions.

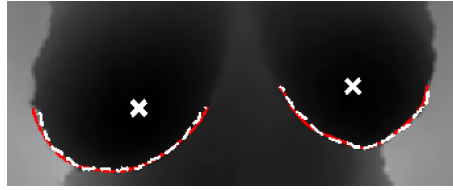


Figure 3.10: Automatic contour detection on depth images from [7] - ground truth (solid red line), detected (dashed white line)

### 3.3 Kinect Sensor as a Tool

The Kinect<sup>TM</sup> is a motion sensing device designed as an hands free game controller for X-BOX 360<sup>TM</sup> video game console. The device has one Red-Green-Blue (RGB) camera and one infrared based depth sensor, both capable of captures at video rate under any ambient lighting conditions with 640x480 pixels. This hardware device is fairly recent and its use has began to widespread in the visual and imaging computer processing community due to its low-cost and applicability potential. Using its sensors the device is capable of rendering a disparity map of the scene on which image processing is applied to recover the 3D data. The collected data from the depth sensor is represented in depth values attributed to each pixel and cannot be transferred directly to real metric distances. However the information present in disparity maps is consistent, therefore comparisons between breast asymmetries or other operations between pixels can be performed, safeguarding the results produced.

By providing 3D data, in the form of disparity maps, it allows the definition of new sets of data inaccessible up to now. Such vital information, as volumetric information, can render the extraction and qualification of new measurements possible to incorporate into the existing BCCT.core model for aesthetic objective evaluation. As demonstrated by Oliveira et al. [14], [6] 3D data extraction using the Kinect<sup>TM</sup> has great potential to introduce volumetric information into BCCT.core system and experiments yielded similar results compared to reference measurements manually performed by a physician. Therefore the software would be greatly improved by the incorporation of 3D data, improving overall aesthetical assessment and for future developments such breast surgery simulations.

Novel approaches on human or scene scanning have been performed using the Kinect<sup>TM</sup> sensor device. Using the colour images combined with the depth maps rendered by the device, Zollhöfer et al. [8] create a high-quality personalized avatar that is designated for home use. The proposed algorithm combines robust non-rigid registration and fitting of a morphable face model to generate a high-quality reconstruction of the facial geometry and texture within seconds (Fig. 3.11).

On [9], the authors describe a method to scan a human body using a single Kinect<sup>TM</sup> by aligning depth and colour scans provided by the device. They achieve a full 360° scan by moving the device freely around the object doing a full rotation in about 30 seconds. To process the data, they apply a 3D SR algorithm followed by a loop-closing method specifically tailored for the Kinect<sup>TM</sup>. Finally they execute non-rigid registration to correct residual errors of movements made. The result is a

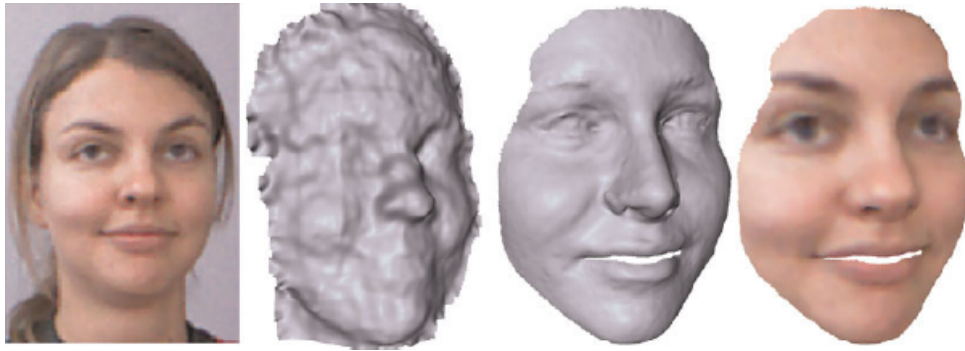


Figure 3.11: Avatar reconstruction process. [8].

complete model with smooth surfaces and very good detailed structures (Fig. 3.12). By using the chosen motion device, the authors add that the main difficulties encountered are the low resolution and low accuracy of the depth sensor, plus its random noise.

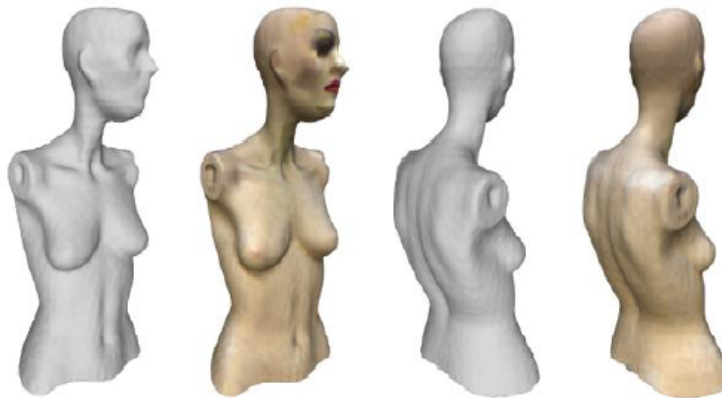


Figure 3.12: Results example of mannequin from Cui and Stricker et al. [9]

In scene scanning and modelling, Henry et al. [10] built 3D dense maps of indoor environments aimed for the use in robotics (Fig. 3.13). They used PrimeSense's camera that is much equivalent to the one installed in Microsoft Kinect<sup>TM</sup> and employ a novel joint optimization algorithm and combine visual features plus shape-based alignment.

Other uses of the device for 3D modelling have been conducted, but all more interesting is the Microsoft's own research group KinectFusion [49]. By using one Kinect<sup>TM</sup> and with hand-held movement, it is possible to reconstruct a high-quality 3D model of the scene. The system captures the scene and for every viewpoint available it renders enhancements onto the model.

As with in [14], [8], [9], [10], the use of disparity maps rendered by the Kinect<sup>TM</sup> to introduce 3D information onto BCCT.core evaluation model that can be very promising. Further, the possibility of using such apparatus is well received by clinicians in favour of too expensive solutions for 3D imaging. Still, this acquisition system may pose difficulties due to its own limitations. Since



Figure 3.13: Surfel update demonstration in Henry et al. [10]. (a) Initial frame; b) Complete updated surfel with 95 RGB-D images.

the system would operate on disparity map images the measurements, and consequently the obtained ratios, are directly related to the pixels on which they were performed. The disparity maps obtained have relatively low-resolution, which may obstruct the construction of reliable models. Therefore the autonomous retrieval of independent breast features suffers from that lack of high-resolution (HR) images. For that reason, the enhancement of the captured images can be essential before their use in later steps in the processing chain.

## Chapter 4

# Super-Resolution Application

### 4.1 Super-Resolution

SR is the process which employs techniques to enhance the resolution of a single or a set of images [50], [51], [52], [53], [54], [55]. The goal of SR is to apply signal processing techniques to increase the spatial resolution and recover details that are present on LR images in aliased form (Fig. 4.1). Due to physical constraints, imaging systems hardware have limitations resulting on a spatial resolution that would not be ideal. Moreover, the costs of HR imaging system are just too high, and also not practical for common use. SR is often seen as an alternative to the usage of such systems, representing a processing stage after image [52].

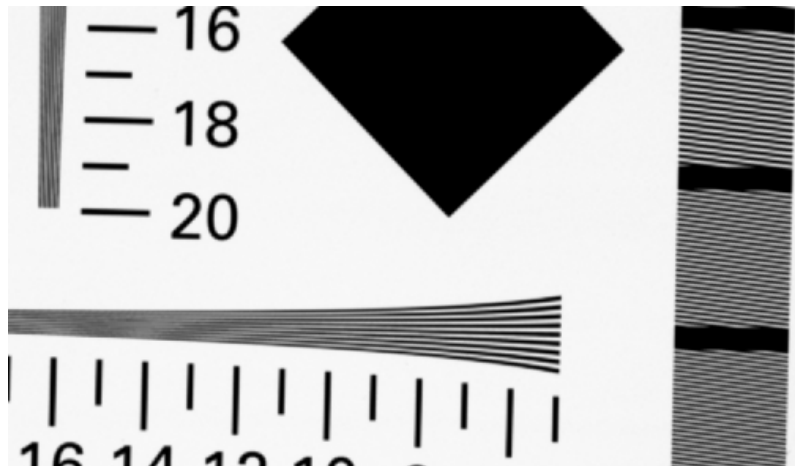


Figure 4.1: Aliasing in high frequency zones in ISO 12233 chart [11].

This segment of signal processing has been under study for several decades, gathering more and more attention with the increase in computational capability verified by today's standards. Authors usually refer to SR as a 3-step process: (1) image registration; (2) image interpolation and (3) image regularization. Some authors call it a 2-step process where they consider that image interpolation and image regularization to be a single normalisation step.

Many times associated with SR is image restoration. Image restoration is applied to recover a degraded image. Most imaging capture devices render LR images, and due to technology limits, these images present blur, noise and aliasing effects. Therefore, part of the enhancement of the captured images is rendered by the elimination of artefacts. For that matter, most SR techniques use image restoration for deblurring and denoising as part of their processing chain.

The registration step corresponds on the motion estimation that is verified in a set of images. This is assuming that there are sub-pixel misalignments, where the aliased information resides. If the shifts are at integer levels, the images would contain the same information, not presenting any gain in detail on the HR image. Also, this step is crucial for the entire process chain. If this step fails to accomplish a very good registration, the entire process is rendered void and a poor, and often very bad, output image is produced. Due to image shifts and the fact that their occurrence is not predictable, the interpolation step is responsible to create a uniformly spaced HR grid through non-uniform interpolation. On this resulting HR image is performed image restoration to remove blur and noise artefacts, resulting in final HR output image.

SR image reconstruction is typically an ill-posed inverse problem and is generally modelled as in (4.1) [55]:

$$y = DHx + v \quad (4.1)$$

where  $y$  is the low resolution image and  $x$  is the unknown high resolution image.  $D$  and  $H$  are degrading operators regarding the downgrading blur and noise present in the images, and  $v$  is additive noise.

The SR methods can be roughly classified into multi-frame, single-frame or example-based variants, either applying algorithms in the frequency or spatial domain. Multi-image methods try to take advantage from the aliased high frequency information that is split across multiple images, while example-based methods consider that it is possible to reconstruct HR information from existing database patches. Single-image methods employ a combination of the other two approaches. They assume that patches can recur inside an image and can be found in the same scale (multi-image) or across different scales (example-based).

Frequency domain algorithms take advantage of redundant information present in the LR images by the shifting and aliasing properties of the Fourier transform, assuming that aliasing has occurred or attempt to extrapolate information to retrieve values within some intervals. Spatial domain algorithms usually employ regularisation based approaches which enable a priori knowledge inclusion, non-uniform interpolation to have the advantage of low computational cost, Projection Onto Convex Sets (POCS) [53] usually designed for simplicity, Iterative Back Projection (IBP) [51], [52] for straightforward implementations, and Maximum A Posteriori (MAP) estimation. The stochastic and example-based approaches also include a priori knowledge or may use the recurrence of patches within images or even the same image.



### 4.1.1 Super-Resolution Applied to Depth Maps

Usually, SR methods were not designed or tested on depth images. But more recently, presumably due to the wider spread of sensors capable of providing depth images, there have been projects using SR and more research into techniques for the specific use of SR in this type of images. Li et al. [56] proposed a multi-frame regularization-based method with new regularization items to yield better results in images with sharp edges and smooth flat regions. Although the performance of the proposed method led to “better results with noise suppression and detail preservation”, experiments were not conducted on depth maps. Moreover on range-enhanced oriented methods, new techniques have been proposed such as [12] reportedly registering enhances of spatial resolution up to 100 times, and [13] using both depth maps and colour images for the increase of resolution being computational efficient when compared to probabilistic approaches. On [12] (Fig. 4.2), the authors propose a method to enhance the resolution by iteratively refine the LR image using HR images as reference. They up-sample the LR input image to the high resolution camera image and process an iteratively refinement over the first image. The refinement module iteratively applies bilateral filtering to each slice of 3D volume of depth probability referred as cost volume. The HR image is obtained by selecting the depth hypothesis with the minimal cost followed by sub-pixel estimation.

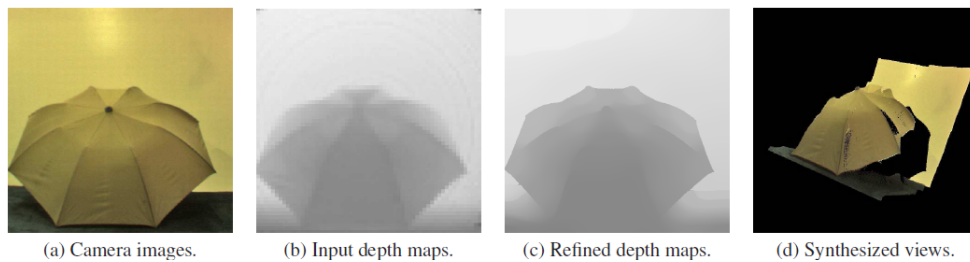


Figure 4.2: Experimental results from Yang et al. [12]

The approach presented in [13], uses an original interpolation technique exploiting side information from a single colour camera image to increase resolution. The proposed method is performed by first pre-processing the colour image through a graph-based segmentation algorithm to identify main surfaces. Then a projection of points of the low resolution depth map is made on the segmented colour image to create a depth grid. The points within each grid are then the initial values of the low resolution depth map. The value of each pixel in the high resolution image is then estimated by interpolation of the grid samples belonging to same regions.

SR presents many advantages with several use cases with successful implementations. In theory, multi-image based methods are able to achieve a substantial increase in detail, but need strict conditions to perform adequately. Most single-image based methods employ stochastic approaches and the inclusion of a priori knowledge. While achieving very good reconstructions, they also take high computational load and may see its performance restrained to the quality of training dictionaries used. The approaches who use redundant information also show good reconstructions



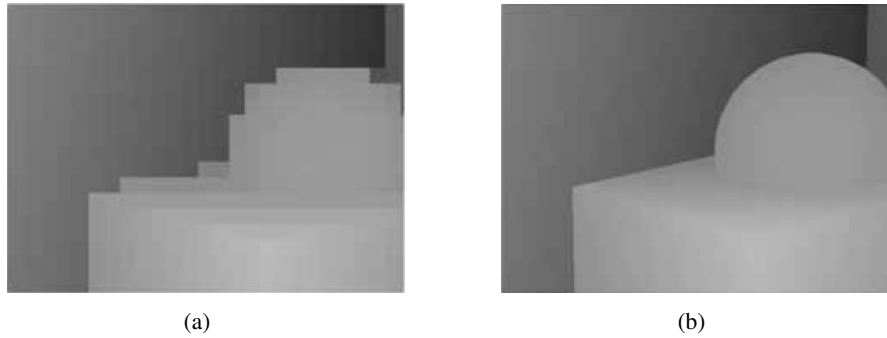


Figure 4.3: Experimental results from Garro et al. [13]. (a) Input image; b) Output image.

without needing a priori knowledge, but have serious limitations if no redundant information exists. Moreover, the cases of SR application on depth maps are very encouraging, and it is hoped to be achieved good outcomes upon this project type of images.

For applicability in BCCT.core SR processing is desired to be at real-time and effective. Also, due to the nature of the rendered LR images, in gray scale, and the necessity to maintain the quality of edges, smooth areas and gradient consistency, SR applicable methods must render and preserve this features properly with minimal degradation. Also, particular attention is given to multi-frame methods since the Kinect<sup>TM</sup> can produce captures at video rate.

## 4.2 Kinect Specification Assessment

By defining the use of the Kinect<sup>TM</sup> device for 3D data acquisition, the knowledge of its operations conditions and technical restrictions is peremptory. The device is capable of operating under any interior lighting conditions, and is a compact and light equipment. The device renders depth maps with 640x480 pixels, but it is further needed to know its range accuracy and depth precision.

An experimental procedure was conducted in order to retrieve the closest capture point and the depth curve according to the distance to the device. It was used Lego<sup>®</sup> blocks, to be set at known positions, as object surfaces. Through various measures, it was verified that the closest point of capture to be around 50 centimetres (cm) from the sensor. Blocks were put every 5 cm apart from each other, and from the 50 cm to the 145 cm mark. It was also put a block with larger dimensions at the distance of 150 cm. This was to facilitate the manual detection of blocks in the depth images, since this block would be identified with ease as it is verified in Figure 4.4(a).

The depth of each block was calculated as the mean value gathered from a sub-block, defined by user input, for every surface block. The depth values are obtained through the denormalization<sup>1</sup> using Equation 4.2, where "dm" is the input depth value and "dr" is the raw depth value previous to normalization performed by the Kinect<sup>TM</sup> drivers used.

<sup>1</sup>[http://groups.google.com/group/openkinect/browse\\_thread/thread/31351846fd33c78/e98a94ac605b9f21?lnk=gst&q=stephane&pli=1](http://groups.google.com/group/openkinect/browse_thread/thread/31351846fd33c78/e98a94ac605b9f21?lnk=gst&q=stephane&pli=1)



Figure 4.4: Kinect<sup>TM</sup> capture setup #2. (a) RGB image; b) Depth image.

$$\sqrt[3]{\frac{dm}{9216}} \times 2047 \equiv dr \quad (4.2)$$

From this point we were able to construct an estimative depth curve for the distances tested as well calculate the mean resolution sensitivity step of distance per depth value (Fig. 4.5). With the registered extreme depth values of 410 and 853, respectively for closer and further blocks, we get a mean step of 0.214 centimetres per depth value (Eq. 4.3).

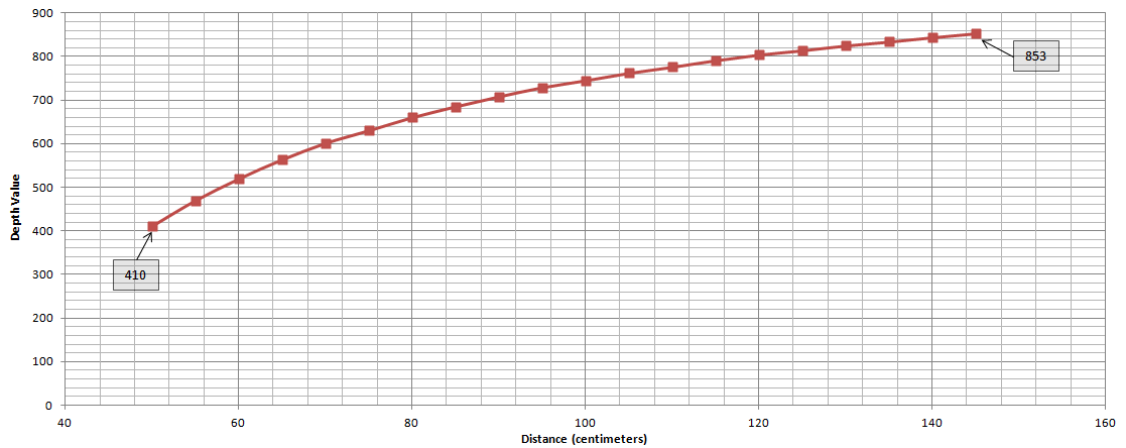


Figure 4.5: Depth Curve.

$$sensitivity = \frac{1450 - 500}{853 - 410} \approx 2.14mm \quad (4.3)$$

As verified in Figure 4.5, the Kinect<sup>TM</sup> renders higher depth resolution the closer the object is to the device. Therefore, the ideal set presented in 4.3 is not constant, where in a close region a given depth range corresponds to a small range of distances, while the same range at a further

distance corresponds to a smaller range of distance values. Likewise, the closer the object is the better would be for the 3D model reconstruction.

In order to study this phenomena and understand the possible implications, a few more experimental setups were explored. In the first, 10 blocks were positioned in the front (starting at 50 cm) and back (starting at 150.9 cm) with 0.3 cm apart from each other. As observed in Figure 4.6, the closer blocks follow a linear tendency with short deviation (Fig. 4.6(a)), compared to the further distant blocks (Fig. 4.6(b)). This evidences that in the back region the linear ideal step is not the actual distance per depth, and the same depth value can correspond to slightly different distance values. Therefore we can not state that the device renders each depth value per 2.14 mm step, while this value may be slightly lower at close distances, but definitely higher at further range.

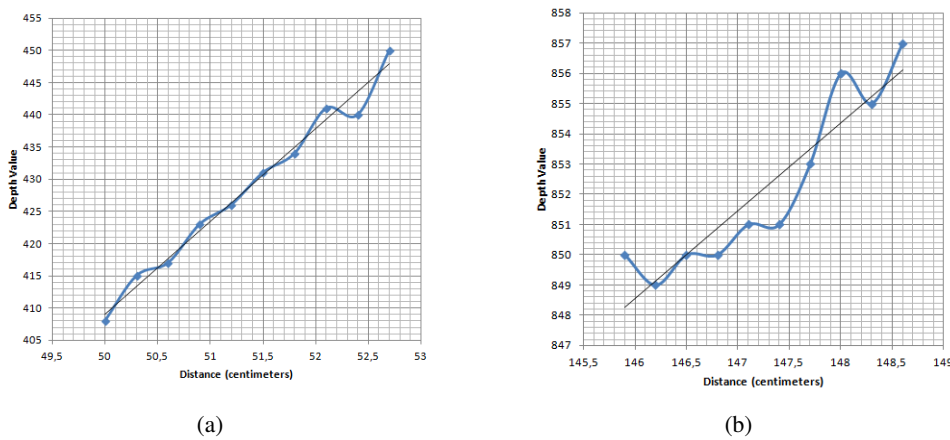


Figure 4.6: Block depth curves. (a) Frontal blocks; b) Rear blocks.

Another experimental procedure was performed, but with the blocks close to each other (no parallel distance) as depicted in Figure 4.7(a). From the ideal step and the previous setup results, it would be expected for the device to provided a repetition of values for the more distant blocks. But that was not the case, instead, the results show an all-round consistency.

The experiment was re-conducted with the blocks 0.2 cm and 0.6 cm apart from each other to verify variations to this data. The corresponding depth curves obtained are represented in Figure 4.8.

From this results, we can conclude that the device is more capable of detecting depths with adjacent objects or within one larger object, than with isolated ones. This is of high significance to us, since the breast shape and the women themselves are one large continuous surface. Also, we can verify that the device fails to provided the same depth at the same distance in different captures. This may be due to imprecisions of the sensors, and the high capability of detecting small variations in close distances, or the opposite, the low capability in far distances. The presence of a pair of the same value at further distance is understandable (Fig. 4.8(e)), with only a 0.2cm distance separating the blocks. Although a high (+3) depth value to on the next step distance. Whether this happens due to sensor limitations or acquisition conditions is unsure.

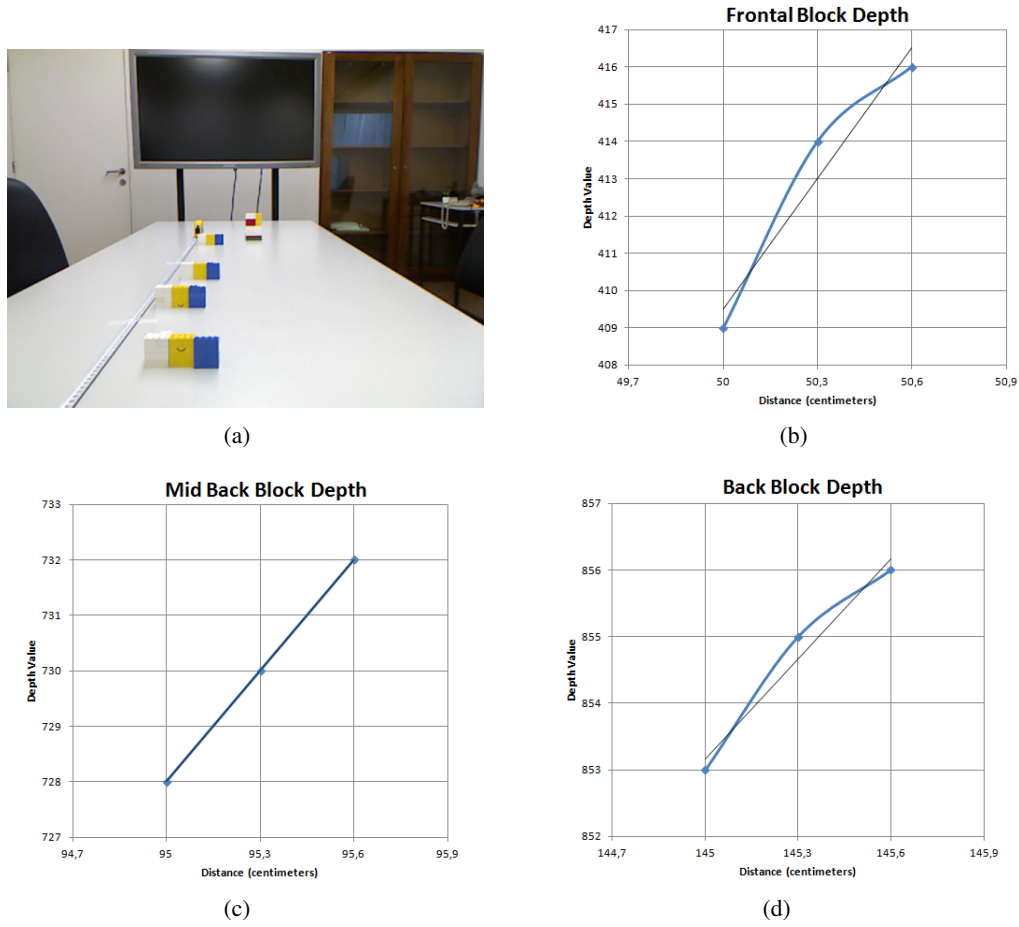
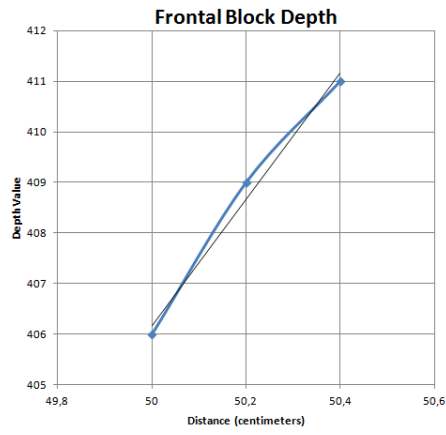


Figure 4.7: Block depth curves. (a) RGB Image; (b) Frontal blocks; (c) Middle blocks; (d) Rear blocks .

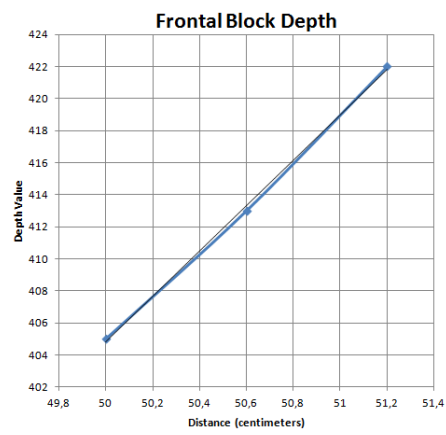
In conclusion, the use of a non-linear model for the distance estimation should improve the consistency, but would be too complex. Besides, the use of such model could prove inaccurate due to slight differences from device to device. For the sake of simplicity, we made use of the Matlab<sup>®</sup> cubic spline data interpolation model (spline function) to calculate the actual distance for the rendered depth based on the data gathered in Figure 4.5. By providing the function values between the known distance intervals, it was proved the function output reliability.

### 4.3 Performance Tests

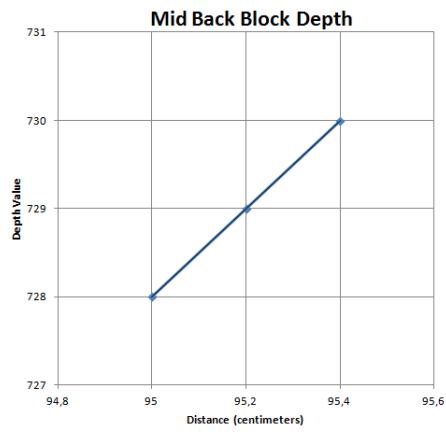
In order to understand the impact of SR application onto this project, firstly, it was needed to test state-of-the-art SR algorithms performance. Eventually, tests are restricted to more recent or updated versions of the accessible implementations. Although this confined the general set of results, it would be impractical to test all implementations that could be found. Not relying on eventual published results for any given algorithm, we have decided to conduct tests with our own



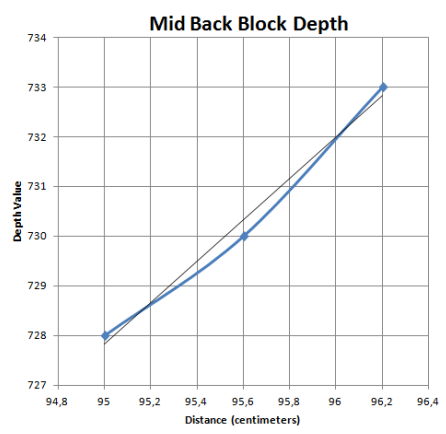
(a)



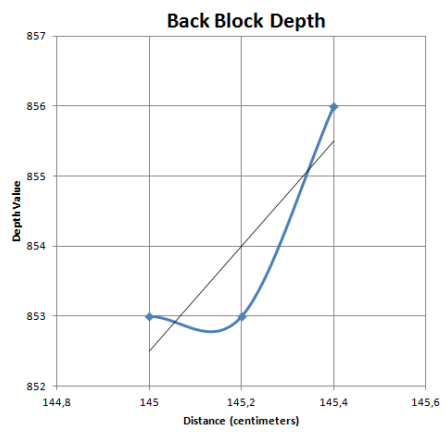
(b)



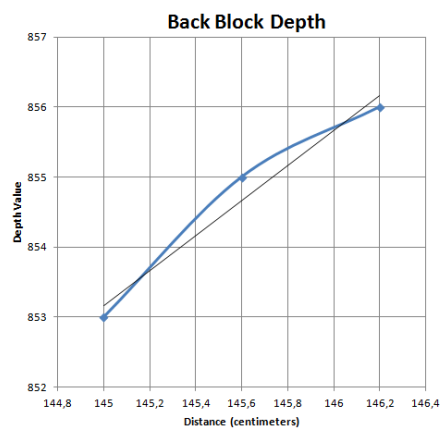
(c)



(d)



(e)



(f)

Figure 4.8: Block depth curves with of blocks spaced 0.2 or 0.6cm. (a) Frontal blocks (0.2cm); b) Frontal blocks (0.6cm); c) Middle blocks (0.2cm); d) Middle blocks (0.6cm); e) Rear blocks (0.2); f) Real blocks (0.6).

images. Then, we are in the position to provide an overview of performance and adaptability over the results, and decide which suits best our needs. In total, eleven programs were tested, ten of which were Matlab<sup>®</sup> implementations and one being a binary executable written in C/C++. Out of the eleven, only six were deemed to execute or produce viable results. Programs were named accordingly to the order they were tested, assuming a nomenclature of "*program#<number>*".

Preliminary experiments were conducted with a total of 12 images, from 3 patients. This comprised a brief study on SR programs' output before proceeding to the available database (Section 4.5.5). A synthetic, gradient-like, image was also put under scrutiny of the tested methods. Due to its linearity, any method should cope far better with it than any other type of image. This was used to confirm the applicability and results. A set of RGB images were also subjected to SR tests, using the available RGB images. 13 colour images were used from 5 patients.

The respective identifiers for each program, author, year, paper, and the web address where they have been fetched are shown in Table 4.1.

## 4.4 Performance Evaluation

For the measurement of performance by each SR method all methods were tested for a scale factor of 2 and, accordingly to their nature, either using single or multi-image based approaches. Some Multi-image based methods were also subjected to sets of images comprising the same image to verify the performance impact of such use case. It is clearly stated when this occurred when presenting the results.

Since we do not hold HR depth images from the scene, the acquired images through the Kinect<sup>™</sup> were our ground truth. Images were acquired manually with the device stationary, with gaps between images of approximately 2 seconds. Then, we downsized those images, with the same scale factor of 2, and then subjected them to SR methods so the final spatial resolution matches the original. Images were downsized assuming a loss of integer pixel information for every 2 pixels, thus not presenting any interpolation that could have impact in the outcome.

All output images were subjected to visual inspection and was registered the Peak Signal to Noise Ratio (PSNR) value to the original image. Most PSNR calculations were taken in a frame size of less 5 pixels in each border of the image. This was due to small artefacts found in images

Table 4.1: Tested Programs

Programs	Info	Web Address
#1	Vandewalle'06 [57]	<a href="http://lcav.epfl.ch/software/superresolution">http://lcav.epfl.ch/software/superresolution</a>
#2	May'11	<a href="http://www.mathworks.com/matlabcentral/fileexchange/33839">http://www.mathworks.com/matlabcentral/fileexchange/33839</a>
#3	Cheng'11	<a href="http://www.mathworks.com/matlabcentral/fileexchange/30488">http://www.mathworks.com/matlabcentral/fileexchange/30488</a>
#4	Hanson'07 [54]	<a href="http://www1.idc.ac.il/toky/videoproc-07/projects/superres/srproject.html">http://www1.idc.ac.il/toky/videoproc-07/projects/superres/srproject.html</a>
#5	Yang'10 [58]	<a href="http://www.ifp.illinois.edu/~jyang29/codes/ScSR.rar">http://www.ifp.illinois.edu/~jyang29/codes/ScSR.rar</a>
#6	Pickup'08 [59]	<a href="http://www.robots.ox.ac.uk/~elle/SRcode/index.html">http://www.robots.ox.ac.uk/~elle/SRcode/index.html</a>
#7	Cheung'06 [60]	<a href="http://www.psi.toronto.edu/~vincent/sourcecode.html">http://www.psi.toronto.edu/~vincent/sourcecode.html</a>
#8	Vandewalle'06 [57]	<a href="http://rr.epfl.ch/3/">http://rr.epfl.ch/3/</a>
#9	Vandewalle'06 [61]	<a href="http://rr.epfl.ch/6/">http://rr.epfl.ch/6/</a>
#10	Dong'11 [55]	<a href="http://www.comp.polyu.edu.hk/~cslzhang/ASDS_AReg.html">http://www.comp.polyu.edu.hk/~cslzhang/ASDS_AReg.html</a>
#11	Dong'09 [62]	<a href="http://www.comp.polyu.edu.hk/~cslzhang/code/NL_Back_projection.zip">http://www.comp.polyu.edu.hk/~cslzhang/code/NL_Back_projection.zip</a>

after resolution enhancement. The PSNR calculation over multi-image based methods output was calculated against the image, of that set, that presented the best linearity in breast contours. This was a limitation over the single-image methods, since no ground truth image would be truthfully known.

For all the experimental procedures in this chapter, Matlab<sup>®</sup> R2011a development environment was used, running on an Intel<sup>®</sup> i5 M450 (@ 2.4 GHz) with 4 GB of RAM memory machine.

## 4.5 Results

### 4.5.1 Depth Images

In a first try-out of the methods to be used, a small number of images were used due to time consuming process of testing with some programs. It was used 4 images from patient #74: (images 071-074) on multi-image methods, and image 074 for single-image methods.

Most methods showed the ability to choose from several registration, motion estimation or reconstruction algorithms, as well as changing some parameters for these steps. Program#1, a Matlab<sup>®</sup> implementation program with a Graphical User Interface (GUI) is an example (Fig. 4.9). Throughout the experiments, some programs were not deemed to run or produce viable results. That is the case of programs #2, #3, #4, #6, #7 and #9, whereas programs #2, #3 and #4 produced undesirable output resolutions and program#7 an output image that did not truly correlates to the original. Besides all efforts, programs #6 and #9 were not able to effectively run, and as with the other programs, were excluded from further tests.

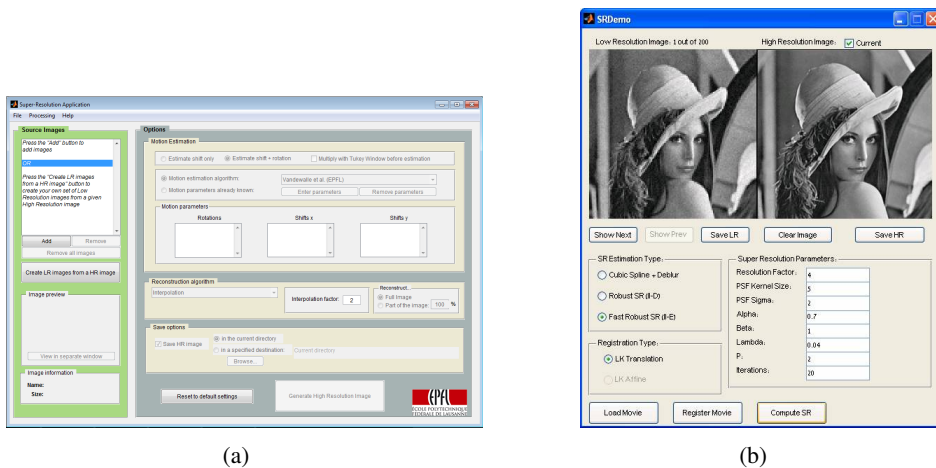


Figure 4.9: Example of programs GUI. a) Program#1 GUI; b) Program#4 GUI.

The remaining programs, #1, #5, #8, #10 and #11 were able to run and produce the expected results. Program#1 made use of several reconstruction methods, while program#5, a single-image based method, made use of dictionaries to improve image reconstruction. Program#8 represented

an updated version of program#9 and used 3 other registration methods (Keren [63], Marcel [64] and Lucchese [65]) for comparison to authors' own method [57].

Finally, programs #10 and #11 were the last to be tested. Program#10 being also a Matlab<sup>®</sup> implementation while #11 is a binary executable. Program#10 made use of internal procedures to simulate a LR image presenting blur and noise. Therefore the provided input image is the original image, and the program was responsible to downgrade this image using the same methodology used in this project. Program#11 was the only binary executable to be tested that was not a Matlab<sup>®</sup> GUI or code-only program. The program's files were in C/C++ language and it was provided all projects material to effectively run it. It accepted single-image inputs of type Portable GrayMap Format (PGM) which was not a limitation for now, since the actual output from the Kinect<sup>™</sup> is given in that file format.

Within the set of programs that did provide usable results, Table 4.2 shows the performance obtained through the application of the SR programs onto the 13 images, as part of the initial trial.

Table 4.2: Performance Trial

Program		#1	#4	#5	#8	#10	#11
PSNR (dB)	Image 074	49.80	35.35	43.59	36.05	51.64	42.40
	Image 083	38.50	42.73	47.12	38.29	53.19	46.00
	Image 112	36.38	32.19	42.28	36.04	49.64	40.80

### 4.5.2 Bounding Box

Despite the tests made over the entire images, it was also of interest to test current methods on images with low dimensions. For that purpose, it was conducted another experimental procedure in which images were cropped to the breasts region. The images used in this test were 074, from patient #7; 083, from patient #8; and image 112, from patient #11.

It is show in Table 4.3 the best result out of the 3 patients.

Table 4.3: Bounding Box Performance Overview

Program	#1	#5	#8	#10	#11
PSNR (db)	39.85	38.80	38.85	49.66	34.00

### 4.5.3 RGB Images

For the automation of BCCT.core and in the interest of using the images captured from the Kinect<sup>™</sup>, the use of RGB images captured by the device may reveal to be extremely beneficial. This would render void the use of a separate HR digital camera. At the start, the low resolution of the RGB images from the Kinect<sup>™</sup> is a serious setback for that scenario. But in the eventuality of the enhancement of these images to be successful, it would be a strong breakthrough. For that reason the study of SR methods on RGB images is needed. The set of best performing methods



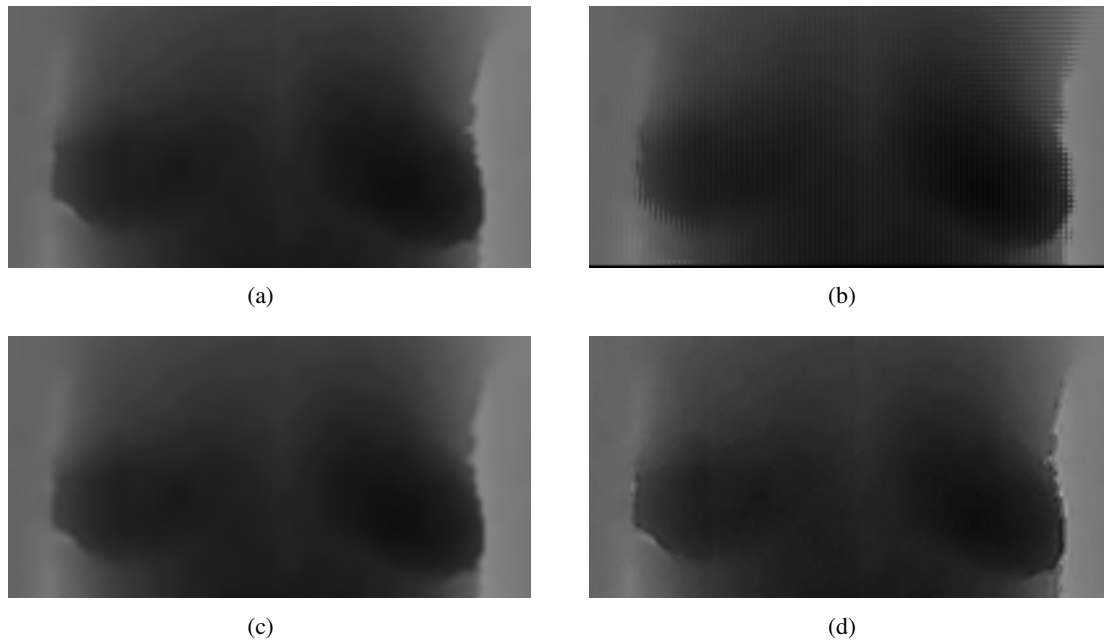


Figure 4.10: Example of Bounding Box SR on image 074. (a) Original; b) Output of program#8; c) Output of program#10; d) Output of program#11.

was tested, using a new set of images, from patient #51 to #55. In total, 13 images were used from the 5 patients.

One last obstacle was imposed by the methods themselves. Some were not able to use colour images (program#11) and while others should have coped with it, they were unable to run with the required images (program#8). Program#11 assumes inputs of 8-bit gray scale images, therefore unable to handle RGB images. While program#8 should cope with RGB images but revealed a processing error while running.

After several efforts, the only output sets came from programs #1, #5 and #10. Results for this experimental procedure are shown in Table 4.4, and their respective output can be visualized in Figure 4.11, where program#1 made use of single-image based input in similarity to programs #5 and #10.

Table 4.4: RGB Performance Overview

Program	#1	#5	#10
Average PSNR (db)	38.57	35.57	38.18

The PSNR value presented was obtained through the average of the individual PSNR channel (Red,Green,Blue). Although not poor results they are clearly inferior than with depth images, most likely due to higher complexity needed to enhance these images.

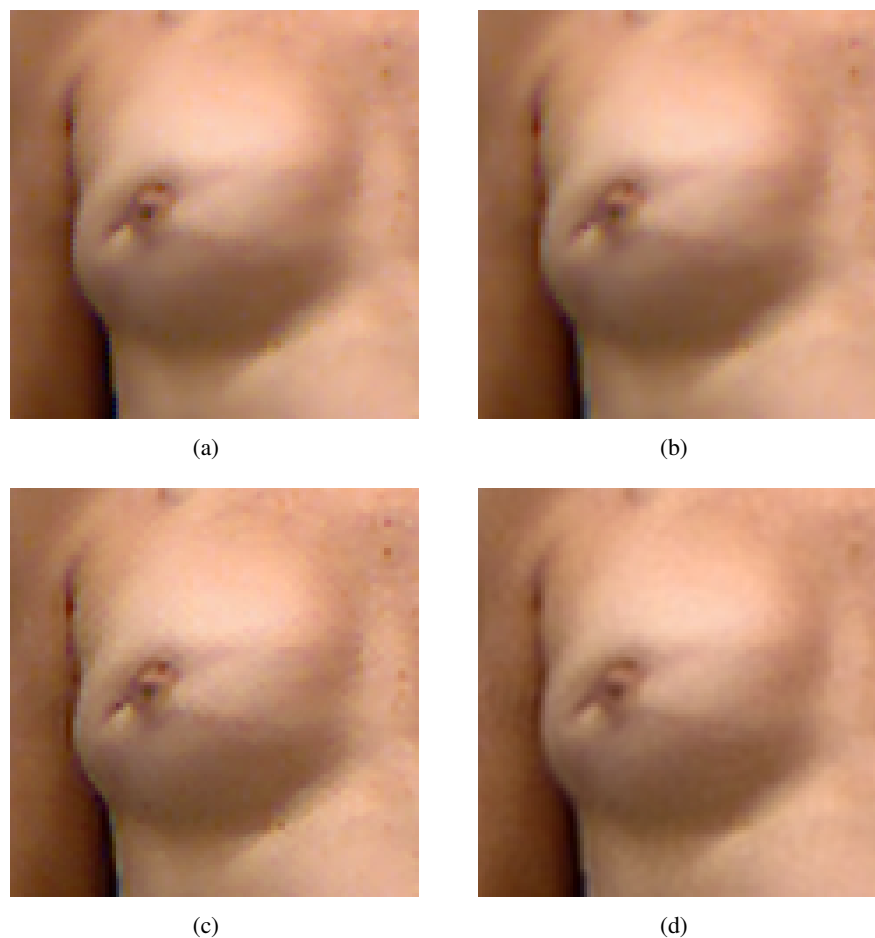


Figure 4.11: Example of application of SR in RGB images (a) Original; b) output of program#1; c) Output of program#5; d) Output of program#10.

#### 4.5.4 Synthetic Images

For the acknowledgement of the tested methods performance a synthetic image was used (Fig. 4.12(a)). The relationship between the outputs provided by each method should confirm the data gathered from the first set of tests, also expecting an increase in performance with this simpler, linear, image.

Tests showed the expected better achievable performance, although with some interesting results. Programs #1 and #8 showed the same result: 50.94 decibels (dB) which did not differentiate any of them in the course of the tests. Program#4 seemed unable to deal with such a linear image and produced an almost black image (registering 5.05 dB). This time, program#5 recorded a better result than #1 and #8 with a PSNR value of 55.05 dB representing a good increase in performance. The best output was still from program#10, with a 70.40 dB PSNR value. Again, it outperformed the remaining methods both in PSNR value and in visual inspection. Table 4.5 shows the obtained results.

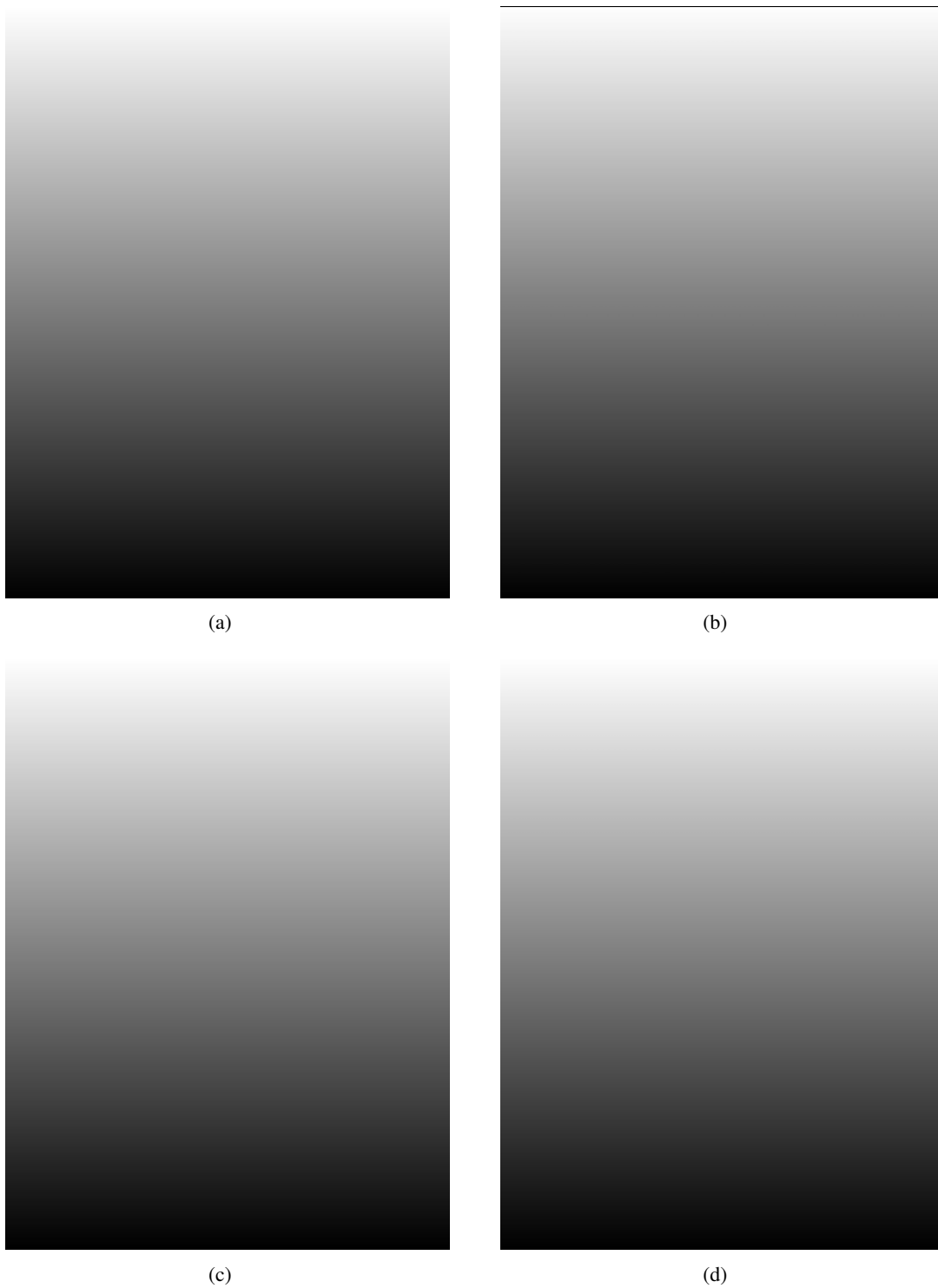


Figure 4.12: Example of application of SR in synthetic images (a) Original; b) output of program#1; c) Output of program#5; d) Output of program#10.

Table 4.5: Synthetic Image Performance Overview

Program	Execution Time (seconds)	PSNR(db)
#1	1.91	50.94
#4	53.48	5.05
#5	358.10	55.05
#8	4.05	50.94
#10	353.75	70.40
#11	5.01	53.2

#### 4.5.5 Extended Set

Posterior to this first stage test phase, we submitted the programs with good outputs to the database of 144 images, comprising 47 patients. This allowed us to test the consistency of each method and identify which would perform best. Results are summarized in Table 4.6. It is shown the average PNSR value obtained for each program and the respective standard deviation. It is also made available the medium execution time to produce a single image. From these results it is clear that program#10 shows the best results. Albeit the processing time would not be the desired, this program presents clear reconstructions above the remaining contenders. Also, it is noted some programs showed similar performance then Matlab<sup>®</sup>'s function "imresize" output, which gathers averages of 41 dB reconstructions.

Table 4.6: Performance Overview

Program	Average Results		Standard Deviation (dB)
	Execution Time (seconds)	PSNR (dB)	
#1	1.61	46.0	0.8
#5	444.42	40.1	1.3
#8	3.00	46.0	0.8
#10	380.99	51.4	1.2
#11	7.35	40.1	1.0

## 4.6 Discussion

Through all the experimentation sets, we verify that we come to interesting results. While we face different results that may vary substantially, we also see a couple of similar results. This may evidence the differences inherent to the application of a determined SR algorithm towards others applying an opposite type of methodology. In some cases, when only the methodology of one processing step is applied, the overall result can be similar to the combination of others. In any case, the general standard deviation throughout the experimentations on the large set of patients is very satisfactory with values to be around plus or minus 1 dB within that method for the depth images. From the general results it is possible to detect the potential of the use of SR methods to

enhance image resolution, before proceeding to further processing. Three programs recorded an average PSNR value above 45 dB, one of which even recorded an average value above 50. This is a very satisfactory reconstruction as confirmed by visual inspection.

Also to note is the fact that multi-image based approaches did not produce the expected results, in most cases, representing a poorer reconstruction in comparison to single-image application, even within the same program. This was attributed to the fact that some images presented a substantial motion, compared to the remaining images of the set. Also, that motion may be big enough to not be at sub-pixel misalignments, therefore the registration step may have compromised the entire process. In order to reach a conclusion on this topic, a clear study should be performed to check if the multi-image based approach may be beneficial in this project application. This would require the source images to be captured within fractions of a second, or noticeably with minor shifts.

## Chapter 5

# Feature Detection

The use of 3D data enables a more complete understanding and renders the aesthetic assessment much more reliable. Although, captured information must be objectively processed and present consistency, as it is needed for an objective assessment. Furthermore, the use of enhanced images provided by SR on depth images can boost the performance to match with real metrics.

It is presented in this Chapter the detection of 3D features, volume, surface area and breast height on the depth images captured with the Kinect<sup>TM</sup> device. It is conducted a study between these features and the real metrics acquired by a medical expert, to conclude on their correlation.

### 5.1 Relevant Measures

Objective techniques for the evaluation of the cosmetic result are based on measurements taken from patients or their representative photographs. These measurements are mostly based on asymmetries between the breasts. Other measurements have been proposed to categorize the breast shape using 3D data, as depicted in Chapter 3, but there is still space for improvements and reach other clinically relevant measures. With the use of 3D data we can obtain these measurements and turn them into parameters for software systems like BCCT.core. Eder et al. [66] defined 8 landmarks further dividing the breast onto 4 quadrants for objective analysis of breast symmetries. Such thorough analysis is rendered relevant due to the fact that surgeons operate based on breast quadrants. Subsequently the calculation of similar regions is in the profound interest to correlate the results with medical experts.

### 5.2 Data Acquisition

The data was acquired with a Kinect<sup>TM</sup> device by a medical expert, under regular clinical environment conditions. Both the captured RGB and depth images were used in experimental procedures. Since both capture lenses are different and slightly misaligned, the resulting images are also misaligned and present distortion. Therefore, a calibration step is required in order to use the same coordinate system in both images. The calibration was performed through the method shown by

Herrera et al. [67], to obtain a coordinate transformation function. Then, we can use the depth images as ground truth for our processing and the RGB images for complementary information.

Automatic breast contour detection is performed over depth images so there is no need to perform a pass through the transformation function. On the contrary, nipples position was extracted using user input on the RGB images and translated into the coordinates of the depth image using the transformation function.

With the breasts contours information it is possible to define a breast mask and plot that data in a 3D mesh plot (Fig. 5.1). Although, before any further processing, it is needed to remove residual errors found in the acquired data. This erroneous data consist of points that exhibit higher depth values than the adjacent ones, and are located on contour regions. This happens due to Kinect<sup>TM</sup>'s Field-of-View (FoV) limitations so there are small non-detected regions, usually found to the right side of the women. To remove this high depth values from the model, we simply project a histogram of the breast mask and remove the points who have peak values outside the mean area. Albeit not a perfect method, it renders satisfactory results without incurring into time expensive operations.

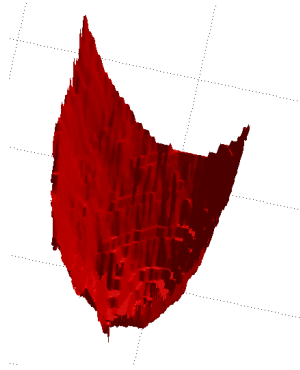


Figure 5.1: 3D plot of breast surface (backwards view).

Patient rotation was also taken into consideration when performing the calculations. It was assumed that the bodies could present some rotation, that would be needed to correct. Body rotation was estimated by using the depth values of points equally distant from a vertical axis that passes through the intermediate point between the breasts' top inner contours points (Fig. 5.2). We compute the rotation based on the mean difference between depth values, and in the case of a rotation being identified, we then convert the data for each side of the vertical axis towards the opposite direction. Finally, the patient is considered to be parallel and ready for processing.

Feature detection and calculation is performed over this, theoretically, error-free data. Volume calculations assumes a dimension in depth values, therefore a change in depth of unitary unit corresponds to the unitary volume. The total volume of each breast is then, defined as the sum of unit values between the body plane and the breast surface limit values. The body plane is considered to be a parallel plane to the camera at the minimum depth that is found in the area between inner breast contours extreme points and the lowest bottom point of breasts (Fig. 5.3). On

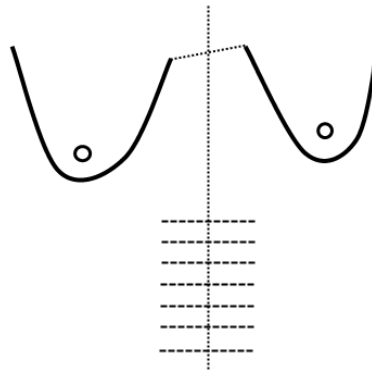


Figure 5.2: Illustration of rotation estimation points.

the other hand, breast surface calculations are extremely complex due to breast geometry. For the retrieval of related area data, it was used the Mathworks<sup>®</sup> code logic<sup>1</sup> to perform the calculation.

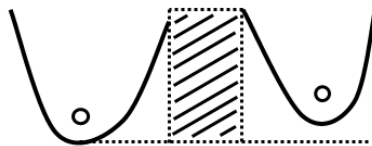


Figure 5.3: Illustration of computable area for plane definition.

For the calculation of breast heights, it was used the same body plane defined for the volume calculations. The depth value of the plane towards the nipple value, represents the clinical relevant measure, considered to be the breast height. This way, we ensure that our calculations are in compliance with the process that the medical expert perform (Fig. 5.4), and we made use of provided data to check for correlations between our results.

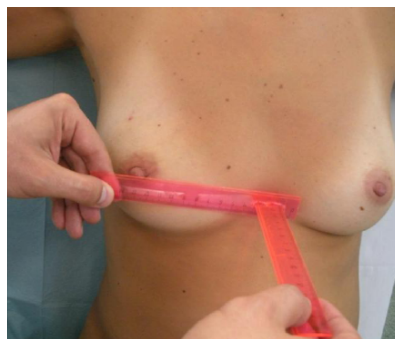


Figure 5.4: Medical expert performing measures.

<sup>1</sup><http://www.mathworks.com/support/solutions/en/data/1-B8O41S/index.html?solution=1-B8O41S>



In this experimental procedure was used a total of 37 images, comprising 11 patients. Depth images used were a normalized version of the raw images rendered by the Kinect<sup>TM</sup> in order to work over the raw depth values. This images have 11-bit depth sensitivity and were wrapped in a 16-bit variable. Both contour and nipple position data was provided, assuming that calibration good was performed.

### 5.3 Tests Results

The relevant data was extracted from the set of patients' images, compiled, and correlated to the given real measures provided.

It is presented in each subsection the measurements results based on the ratio between the treated and the non-treated breast, alongside the respective average standard deviation. The procedure was replicated for the enhanced images, but only a few programs were capable of producing output images from the normalized raw images provided by the Kinect<sup>TM</sup>. Programs #5, #8 and #10 were perfectly able to produce output images, while program#1 produced an image with almost zero values, while program#11 only accepted images represented in 8-bit. Besides all efforts, the modification of program#10 was not successful in order to make it render an image of times two (x2) the initial resolution. Therefore, the only available test outputs of program#5 and #8 were used.

Also, these restrictions took place in order to use the raw image without rescaling it to fill the range of the 16-bit variables. Future use of the data may lift this restriction to which may render program#1 able to produce an image.

#### 5.3.1 Volume

Volume information per patient without rotation estimation is summarized in Table 5.1, while the results employing rotation estimation are shown in Table 5.2. Volume ratio is calculated from the higher breast volume value over the low volume value. For comparison purposes it is indicated the ratio of breast heights provided by medical experts' real measurements and the ratios calculated over the enhanced images of programs #5 and #8. Figure 5.5 shows a scatter plot of points ratio relationship with the correspondent tendency line. This graphical visualization shows best the relationship between values.

Table 5.1: Volume Data Without Rotation Compensation

Patient#	Real Height Ratio	Volume Ratios	Standard Deviation	Program#5 Volume Ratio	Standard Deviation	Program#8 Volume Ratio	Standard Deviation
52	1.077	1.051	0.022	1.045	0.014	1.042	0.014
54	1.353	1.023	0.020	1.046	0.034	1.044	0.035
55	1.190	1.110	0.099	1.095	0.092	1.090	0.091
68	1.417	1.089	0.019	1.070	0.039	1.079	0.040
73	1.091	1.031	0.036	1.028	0.028	1.029	0.030
74	1.245	1.152	0.045	1.131	0.035	1.130	0.043
75	1.152	1.038	0.027	1.046	0.033	1.056	0.034
76	1.000	1.040	0.022	1.044	0.020	1.046	0.018
77	1.234	1.023	0.012	1.029	0.016	1.033	0.008
78	1.478	1.208	0.066	1.193	0.061	1.193	0.060
79	1.056	1.132	0.024	1.114	0.024	1.109	0.024

Table 5.2: Volume Data With Rotation Compensation

Patient#	Real Height Ratio	Volume Ratios	Standard Deviation	Program#5 Volume Ratio	Standard Deviation	Program#8 Volume Ratio	Standard Deviation
52	1.077	1.064	0.025	1.060	0.016	1.056	0.017
54	1.353	1.038	0.011	1.066	0.019	1.066	0.018
55	1.190	1.061	0.059	1.072	0.060	1.067	0.060
68	1.417	1.090	0.021	1.066	0.033	1.073	0.037
73	1.091	1.031	0.036	1.028	0.028	1.028	0.028
74	1.245	1.075	0.056	1.060	0.049	1.056	0.049
75	1.152	1.032	0.019	1.024	0.015	1.029	0.016
76	1.000	1.045	0.020	1.049	0.026	1.051	0.026
77	1.234	1.023	0.012	1.029	0.016	1.033	0.008
78	1.478	1.199	0.054	1.193	0.061	1.181	0.078
79	1.056	1.132	0.024	1.066	0.050	1.061	0.051

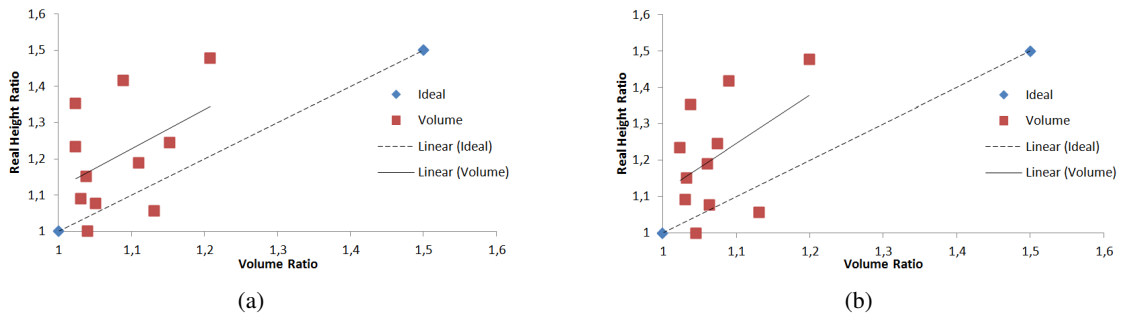


Figure 5.5: Scatter plot of volume ratios. a) Without rotation compensation; b) With rotation compensation.

### 5.3.2 Surface Area

In this section it is presented the results for surface area ratios. Notwithstanding the fact that these results were obtained from the application of an external algorithmic procedure, it is still relevant to compare them with the remaining ratios gathered. Table 5.3 and Table 5.4 show the obtained ratios with and without rotation compensation, respectively. A scatter plot of points ratio relationship can be found in Figure 5.6.

Table 5.3: Area Data Without Rotation Compensation

Patient#	Real Height Ratio	Area Ratios	Standard Deviation	Program#5 Area Ratio	Standard Deviation	Program#8 Area Ratio	Standard Deviation
52	1.077	1.079	0.025	1.103	0.040	1.056	0.023
54	1.353	1.030	0.040	1.035	0.016	1.027	0.035
55	1.190	1.107	0.100	1.108	0.091	1.085	0.094
68	1.417	1.100	0.044	1.163	0.071	1.099	0.057
73	1.091	1.040	0.059	1.057	0.055	1.040	0.041
74	1.245	1.154	0.046	1.094	0.032	1.101	0.040
75	1.152	1.061	0.046	1.079	0.037	1.084	0.039
76	1.000	1.043	0.028	1.080	0.048	1.039	0.049
77	1.234	1.045	0.028	0.017	0.016	1.028	0.024
78	1.478	1.197	0.076	1.190	0.058	1.190	0.053
79	1.056	1.132	0.020	1.109	0.030	1.103	0.026

Table 5.4: Area Data With Rotation Compensation

Patient#	Real Height Ratio	Area Ratios	Standard Deviation	Program#5 Area Ratio	Standard Deviation	Program#8 Area Ratio	Standard Deviation
52	1.077	1.099	0.025	1.156	0.033	1.074	0.026
54	1.353	1.046	0.027	1.023	0.010	1.053	0.015
55	1.190	1.064	0.043	1.086	0.063	1.066	0.066
68	1.417	1.102	0.045	1.150	0.065	1.088	0.050
73	1.091	1.040	0.059	1.057	0.055	1.039	0.039
74	1.245	1.069	0.054	1.033	0.007	1.039	0.014
75	1.152	1.039	0.014	1.037	0.023	1.039	0.032
76	1.000	1.046	0.022	1.095	0.061	1.057	0.049
77	1.234	1.045	0.028	1.017	0.016	1.028	0.024
78	1.478	1.188	0.064	1.190	0.058	1.171	0.085
79	1.056	1.132	0.020	1.060	0.050	1.056	0.051

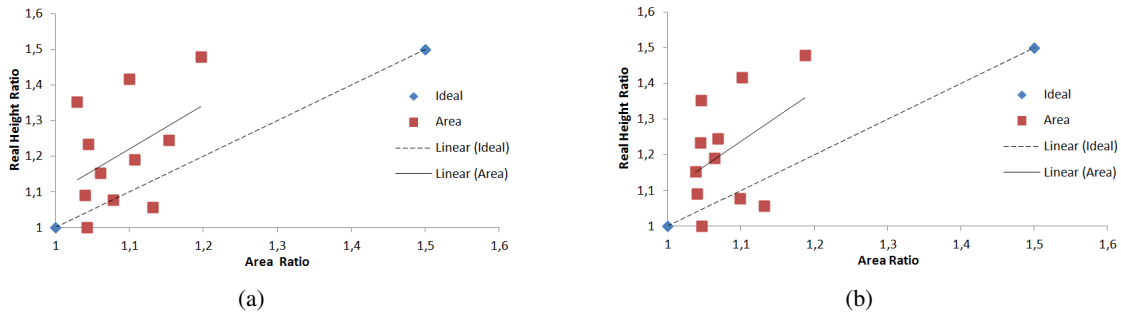


Figure 5.6: Scatter plot of area ratios. a) Without rotation compensation; b) With rotation compensation.

### 5.3.3 Breast Height

Much to the resemblance to previous sections, it is presented in this section the results for height ratios calculations. As previously explained, these heights are based on a defined body plane towards nipple position. The Kinect<sup>TM</sup> depth step assessment made possible to translate the heights, in depth context, to real metric values, making possible to test if the depth-to-metric estimation would be precise. Therefore, it was possible to calculate heights ratio based on these translated

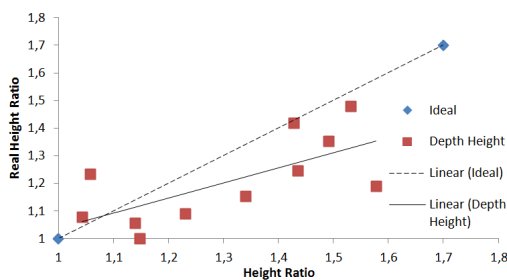
values, and check if they represent any improvement or are compatible with real metrics provided. Table 5.5 and Table 5.6 show the height ratios for depth height values, and Figures 5.7(a) and 5.7(b) the corresponding plot and tendency line.

Table 5.5: Depth Height Data Without Rotation Compensation

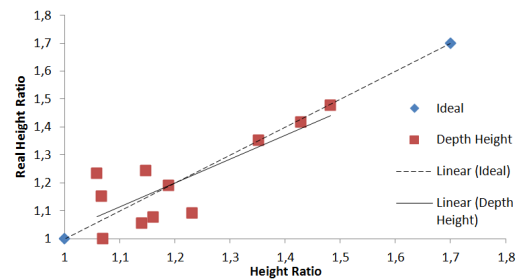
Patient#	Real Height Ratio	Height Ratios	Standard Deviation	Program#5 Height Ratio	Standard Deviation	Program#8 Height Ratio	Standard Deviation
52	1.077	1.044	0.042	1.044	0.042	1.042	0.042
54	1.353	1.492	0.249	1.454	0.203	1.417	0.189
55	1.190	1.578	0.211	1.578	0.211	1.158	0.177
68	1.417	1.429	0.000	n/a	n/a	n/a	n/a
73	1.091	1.232	0.041	1.232	0.041	1.248	0.062
74	1.245	1.436	0.044	1.425	0.039	1.401	0.054
75	1.152	1.340	0.191	1.340	0.191	1.394	0.200
76	1.000	1.148	0.005	1.148	0.005	1.148	0.005
77	1.234	1.059	0.000	1.052	0.006	1.125	0.000
78	1.478	1.532	0.160	1.525	0.169	1.532	0.160
79	1.056	1.140	0.082	1.120	0.087	1.063	0.080

Table 5.6: Depth Height Data With Rotation Compensation

Patient#	Real Height Ratio	Height Ratios	Standard Deviation	Program#5 Height Ratio	Standard Deviation	Program#8 Height Ratio	Standard Deviation
52	1.077	1.161	0.081	1.188	0.097	1.153	0.066
54	1.353	1.352	0.140	1.322	0.095	1.295	0.102
55	1.190	1.189	0.110	1.445	0.023	1.345	0.017
68	1.417	1.429	0.000	n/a	n/a	n/a	n/a
73	1.091	1.232	0.041	1.232	0.041	1.222	0.106
74	1.245	1.148	0.107	1.148	0.107	1.121	0.064
75	1.152	1.067	0.078	1.067	0.078	1.098	0.066
76	1.000	1.069	0.002	1.069	0.002	1.069	0.002
77	1.234	1.059	0.000	1.052	0.006	1.125	0.000
78	1.478	1.483	0.226	1.525	0.169	1.461	0.045
79	1.056	1.140	0.082	1.122	0.101	1.104	0.131



(a)



(b)

Figure 5.7: Scatter plot of depth height ratios. a) Without rotation compensation; b) With rotation compensation.

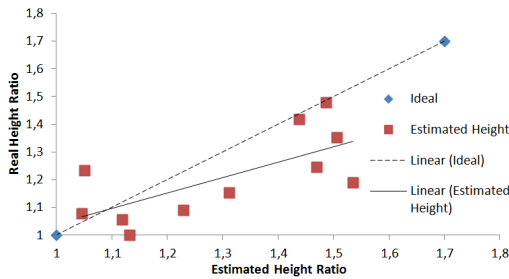
Following the same experimental procedures, depth values were converted to metric values, and then computed the estimated height ratios. The results are summarize in Table 5.7 and 5.8, and Figure 5.8 shows the relationship to the real metric values.

Table 5.7: Estimated Height Data Without Rotation Compensation

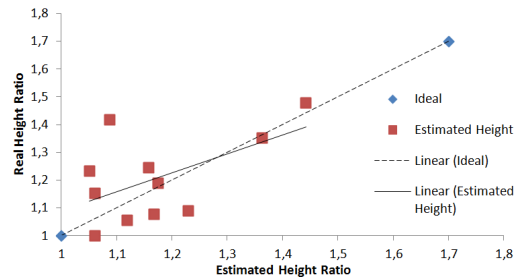
Patient#	Real Height Ratio	Height Ratios	Standard Deviation	Program#5 Height Ratio	Standard Deviation	Program#8 Height Ratio	Standard Deviation
52	1.077	1.046	0.044	1.046	0.044	1.044	0.044
54	1.353	1.506	0.251	1.467	0.205	1.429	0.188
55	1.190	1.535	0.198	1.535	0.198	1.425	0.166
68	1.417	1.439	0.196	n/a	n/a	n/a	n/a
73	1.091	1.230	0.042	1.230	0.042	1.246	0.061
74	1.245	1.470	0.051	1.457	0.043	1.433	0.061
75	1.152	1.312	0.174	1.312	0.174	1.360	0.182
76	1.000	1.133	0.005	1.133	0.005	1.133	0.005
77	1.234	1.051	0.001	1.045	0.005	1.109	0.001
78	1.478	1.487	0.148	1.480	0.157	1.487	0.148
79	1.056	1.120	0.070	1.103	0.073	1.054	0.069

Table 5.8: Estimated Height Data With Rotation Compensation

Patient#	Real Height Ratio	Estimated Height Ratios	Standard Deviation	Program#5 Height Ratio	Standard Deviation	Program#8 Height Ratio	Standard Deviation
52	1.077	1.168	0.084	1.197	0.100	1.160	0.068
54	1.353	1.363	0.138	1.333	0.094	1.303	0.099
55	1.190	1.175	0.102	1.412	0.023	1.310	0.017
68	1.417	1.088	0.196	n/a	n/a	n/a	n/a
73	1.091	1.230	0.042	1.230	0.042	1.220	0.106
74	1.245	1.158	0.115	1.158	0.115	1.130	0.070
75	1.152	1.061	0.071	1.061	0.071	1.090	0.060
76	1.000	1.061	0.002	1.061	0.002	1.061	0.002
77	1.234	1.051	0.001	1.045	0.005	1.109	0.001
78	1.478	1.442	0.208	1.480	0.157	1.422	0.043
79	1.056	1.120	0.070	1.105	0.087	1.089	0.113



(a)



(b)

Figure 5.8: Scatter plot of estimated metric height ratios. a) Without rotation compensation; b) With rotation compensation.

## 5.4 Discussion

With the processing of the 3D data acquired through a low-cost apparatus, it is confirmed the possibility to detect features and extract information about the breast shape. We have come to very interesting results that show the usage of a Kinect<sup>TM</sup> device onto the BCCT evaluation to be very promising, and achieve close results from ground truth obtained by a medical expert. When comparing height measures directly, we verify that a compensation of rotation improves significantly

the results with several pair of ratios to be identical. Moreover, the estimated metric measurements are very much similar. This can make clinical experts to prove the measures obtained by the software, and render possible to use the data for simulation of interventions.

Although in some cases there was verified a moderate difference, the overall performance is very good. Interfering in the data, may be smaller patients' breasts or too similar breast shapes since the smaller the ratios are, the more errors we find towards real values.

When comparing volume and area data, we find a natural difference towards height ratios, albeit the results show an interesting tendency. The lack of real metric information does not let us conclude any further.

The application of SR methods towards raw base images, may seem to produce similar results at first glance, specially with volume and area data. But when we plot the height data we verify that some differences arise. In fact, when no rotation compensation is applied the results are identical to those obtained with raw images, both using programs' #5 and #8 outputs (Fig. 5.9).

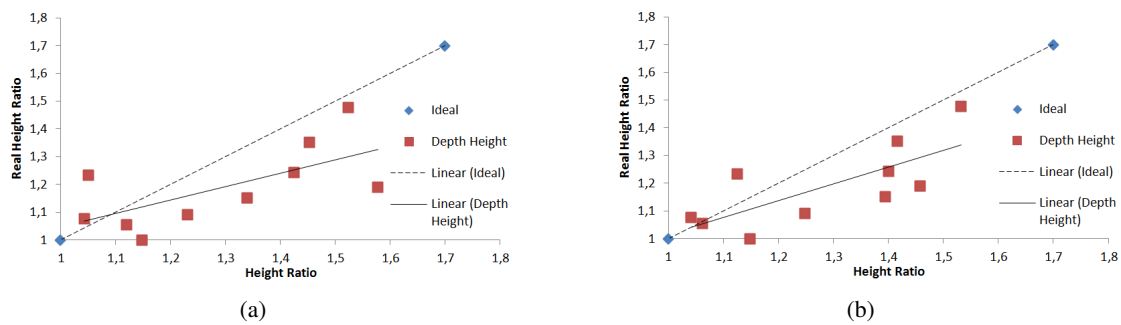


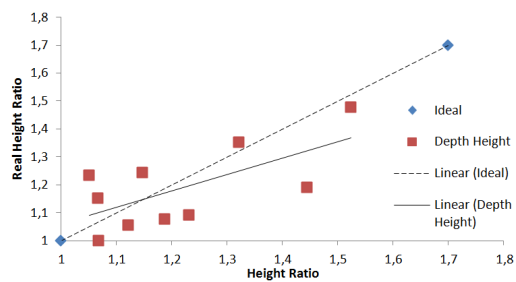
Figure 5.9: Scatter plot of height ratios (no rotation compensation). a) From program#5 output; b) From program#8 output.

But when rotation compensation is performed, program#8 (Fig. 5.10(b)) shows similar tendency to original images under the same condition (Fig. 5.7(b)), while program#5 evidences a clear less in result tendency towards ideal ratio (Fig. 5.10(a)). To support the observable results, the same behaviour is seen in the correlation of values between original data and from the one taken from enhanced images, as shown in Table 5.9.

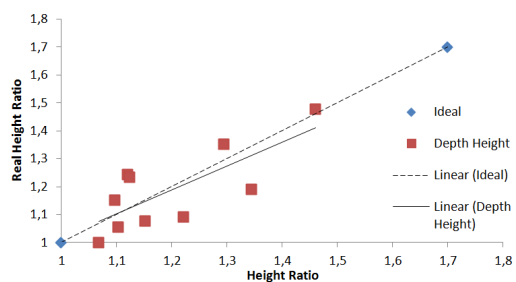
Table 5.9: Correlation of height ratios between LR and HR images.

Program#	Correlation	
	No Rotation Compensation	With Rotation Compensation
#5	0.9982	0.8648
#8	0.9583	0.8909

Although the results found in enhanced images by program#8 indicate a slight deformation in detail, this can only be confirmed with a more extensive database.



(a)



(b)

Figure 5.10: Scatter plot of height ratios after rotation compensation. a) From program#5 output; b) From program#8 output.

## Chapter 6

# Conclusions and Future Work

### 6.1 Conclusions

The work presented in this document shows a study on the application of low-cost equipment, namely the Kinect<sup>TM</sup> device, to detect 3D features. For that purpose, an initial study of SR methods applicability was conducted. Although, the study was limited to the publicly available programs, the general output images were considered to be fairly good. Nonetheless, due to the lack of availability of open SR solutions it could not be studied state-of-the-art methods specifically tailed for depth images. Therefore, a true knowledge of the performance they could achieve on this projects' images is unknown.

Furthermore, the application of SR onto this project's RGB images may be considered standard. But their use in BCCT.core software needs to be studied in order to render unnecessary the use of a HR digital camera. Also, single-image based methods provided the best results. The database of input images may show inappropriate for multi-image methods, so there is a need to study the required characteristics and if they can be acquired through the device or alter the process of acquisition to render more consecutive images. The use of SR methods onto the raw depth images did not provided the expected improvement, much to the success of the data gathered from the original images. Thus, no beneficial gain was verified. Nevertheless, the data provided by enhanced images through are identical.

The reconstructed 3D models were sufficient, but other techniques have been applied in order to render better approximation models [9], [49], [10]. The introduction of these enhanced models could provided better results than the use of the statically acquired model. Also, the SR application onto other processing chain may render higher and valuable significance.

Lastly, it is verified that from the acquired 3D data it is possible to reach identical height measures than the ones performed by a medical expert. Other measures were obtained, but their relevance towards their respective real metrics must be acquainted. Then, it is possible to state that the use of such low-cost equipment can render approximate models to extract clinical relevant measures.



## 6.2 Future Work

From the conclusions of this project, there is a set of unresolved topics that still need to be addressed. Either to achieve improvements onto the BCCT evaluation or to BCCT.core software, the relevant actions should be performed:

- Study the application of enhanced RGB images from the Kinect<sup>™</sup> onto BCCT.core system;
- Study the importance of acquisition methodologies for Multi-image SR methods;
- Test the performance of enhanced images making use of tailored SR methods;
- The acquaintance of real metric models for ground truth comparison towards more measures;
- Comparative study of the 2D measures between BCCT.core and the use of a 3D model;
- Comparative study of 3D breast quadrant measures towards ground truth, or medical reference measures;
- Come to the definition of new 3D measures for the evaluation of BCCT.

# References

- [1] Giovanni Maria Farinella, Gaetano Impoco, Giovanni Gallo, Salvatore Spoto, and Giuseppe Catanuto. Unambiguous analysis of woman breast shape for plastic surgery outcome evaluation. In *Eurographics Italian Chapter Conference*, pages 255–261, 2006.
- [2] R. Balaniuk, I. Costa, and J. Mello. Cosmetic breast surgery simulation. In *SVR2006 VIII Symposium on Virtual Reality*, pages 387–396, 2006.
- [3] G. Catanuto, A. Spano, A. Pennati, E. Riggio, G.M. Farinella, G. Impoco, S. Spoto, G. Gallo, and M.B. Nava. Experimental methodology for digital breast shape analysis and objective surgical outcome evaluation. *Journal of Plastic, Reconstructive & Aesthetic Surgery*, 61(3):314 – 318, 2008.
- [4] Jaime S. Cardoso, Ricardo Sousa, Luis F. Teixeira, and Maria J. Cardoso. Breast contour detection with stable paths. In A. Fred, J. Filipe, and H. Gamboa, editors, *Biomedical Engineering Systems and Technologies*, volume 25 of *Communications in Computer and Information Science*, pages 439–452. Springer-Verlag Berlin Heidelberg, 2009.
- [5] H. P. Oliveira, A. Magalhaes, M. J. Cardoso, and J. S. Cardoso. Improving the bcct.core model with lateral information. In *Proceedings of the 10<sup>th</sup> IEEE International Conference on Information Technology and Applications in Biomedicine*, pages 1–4, 2010.
- [6] Helder Oliveira, Andre Magalhaes, and Jaime S. Cardoso. Kinect based method for the bcct quantitative 3d evaluation. In *Proceedings of 17th Portuguese Conference on Pattern Recognition (RECPAD)*, 2011.
- [7] Helder P. Oliveira, Jaime S. Cardoso, Andre Magalhaes, and Maria J. Cardoso. Simultaneous detection of prominent points on breast cancer conservative treatment images. In *Proceedings of The IEEE International Conference on Image Processing (ICIP)*, 2012.
- [8] Michael Zollhofer, Michael Martinek, Gunther Greiner, Marc Stamminger, and Jochen SuB-muth. Automatic reconstruction of personalized avatars from 3d face scans. *Comput. Animat. Virtual Worlds*, 22(2-3):195–202, April 2011.
- [9] Yan Cui and Didier Stricker. 3d body scanning with one kinect. In *2nd International Conference on 3D Body Scanning Technologies*, 10 2011.
- [10] P. Henry, M. Krainin, E. Herbst, X. Ren, and D. Fox. RGB-D Mapping: Using depth cameras for dense 3D modeling of indoor environments. In *Proceedings of the 12th International Symposium on Experimental Robotics*, 2010.
- [11] Iso 12233:2000. *Photography - Electronic still-picture cameras - Resolution measurements*. International Organization for Standardization (ISO), Geneva, Switzerland, 2000.

- [12] Qingxiong Yang, Ruigang Yang, James Davis, and David Nister. Spatial-depth super resolution for range images. In *In CVPR, 2007*. 8, 2007.
- [13] Valeria Garro, Pietro Zanuttigh, and Guido M. Cortelazzo. A new super resolution technique for range data. In *In Proceedings of GTTI Meeting 2009, Parma, Italy*, 2009.
- [14] H. P. Oliveira, P. Patete, G. Baroni, and J. S. Cardoso. Development of a bcct quantitative 3d evaluation system through low-cost solutions. In *Proceedings of the 2<sup>nd</sup> International Conference on 3D Body Scanning Technologies*, pages 16–27, 2011.
- [15] Ahmedin Jemal, Freddie Bray, Melissa M. Center, Jacques Ferlay, Elizabeth Ward, and David Forman. Global cancer statistics. *CA: A Cancer Journal for Clinicians*, 61(2):69–90, 2011.
- [16] B. Fisher, S. Anderson, J. Bryant, R. G. Margolese, M. Deutsch, E. R. Fisher, J. H. Jeong, and N. Wolmark. Twenty-year follow-up of a randomized trial comparing total mastectomy, lumpectomy, and lumpectomy plus irradiation for the treatment of invasive breast cancer. *the New England Journal of Medicine*, 347:1233–1241, 2002.
- [17] Janet Polivy. Effects of radical mastectomy on a woman’s feminine self-concept. In *Northwestern University, Evanston, Illinois*, 1972.
- [18] U. Veronesi, N. Cascinelli, L. Mariani, M. Greco, R. Saccozzi, A. Luini, M. Aguilar, and E. Marubini. Twenty-year follow-up of a randomized study comparing breast-conserving surgery with radical mastectomy for early breast cancer. *the New England Journal of Medicine*, 347:1227–1232, 2002.
- [19] M. R. Christiaens, E. van der Schueren, and K. Vantongelen. More detailed documentation of operative procedures in breast conserving treatment: what good will it do us? *European Journal of Surgical Oncology*, 22:326–330, 1996.
- [20] I Fentiman and M Christiaens. Quality assurance of surgery in clinical trials. *Eur J Cancer*, 30A(2):136 – 137, 1994.
- [21] J. R. Harris, M. B. Levene, G. Svensson, and S. Hellman. Analysis of cosmetic results following primary radiation therapy for stages i and ii carcinoma of the breast. *Int. Journal of Radiation Oncology Biology Physics*, 5:257–261, 1979.
- [22] V. Sacchini, A. Luini, S. Tana, L. Lozza, V. Galimberti, M. Merson, R. Agresti, P. Veronesi, and M. Greco. Quantitative and qualitative cosmetic evaluation after conservative treatment for breast cancer. *European Journal Cancer*, 27:1395–1400, 1991.
- [23] D. R. H. Christie, M-Y. O’Brien, J. A. Christie, T. Kron, S. A. Ferguson, C. S. Hamilton, and J. W. Denham. A comparison of methods of cosmetic assessment in breast conservation treatment. *Breast*, 5:358–367, 1996.
- [24] E. V. Limbergen, E. V. Schueren, and K. V. Tongelen. Cosmetic evaluation of breast conserving treatment for mammary cancer. 1. proposal of a quantitative scoring system. *Radiotherapy and Oncology*, 16:159–167, 1989.
- [25] S. K. Al-Ghazal, R. W. Blamey, J. Stewart, and A. L. Morgan. The cosmetic outcome in early breast cancer treated with breast conservation. *European Journal of Surgical Oncology*, 25:566–570, 1999.

- [26] R. D. Pezner, M. P. Patterson, L. R. Hill, N. Vora, K. R. Desai, J. O. Archambeau, and J. A. Lipsett. Breast retraction assessment: an objective evaluation of cosmetic results of patients treated conservatively for breast cancer. *International Journal of Radiation Oncology Biology Physics*, 11:575–578, 1985.
- [27] Maximilian Eder, Fee v. Waldenfels, Alexandra Swobodnik, Markus Kloppel, Ann-Kathrin Pape, Tibor Schuster, Stefan Raith, Elena Kitzler, Nikolaos A. Papadopoulos, Hans-Gunther Machens, and Laszlo Kovacs. Objective breast symmetry evaluation using 3-d surface imaging. *The Breast*, 21(2):152 – 158, 2012.
- [28] J. S. Cardoso and M. J. Cardoso. Towards an intelligent medical system for the aesthetic evaluation of breast cancer conservative treatment. *Artificial Intelligence in Medicine*, 40:115–126, 2007.
- [29] M. J. Cardoso, A. C. Santos, Jaime S. Cardoso, H. Barros, and M. C. Oliveira. Choosing observers for evaluation of aesthetic results in breast cancer conservative treatment. *International Journal of Radiation Oncology, Biology and Physics*, 61:879–881, 2005.
- [30] Jaime S. Cardoso, Joaquim F. Pinto da Costa, and Maria J. Cardoso. Modelling ordinal relations with SVMs: an application to objective aesthetic evaluation of breast cancer conservative treatment. *Neural Networks*, 18:808–817, june-july 2005.
- [31] F. Fitzal, W. Krois, H. Trischler, L. Wutzel, O. Riedl, U. Kuhelbock, B. Wintersteiner, M.J. Cardoso, P. Dubsky, M. Gnant, R. Jakesz, and T. Wild. The use of a breast symmetry index for objective evaluation of breast cosmesis. *The Breast*, 16(4):429–435, 2007.
- [32] Maria J. Cardoso, Jaime S. Cardoso, Thomas Wild, Wilfried Krois, and Florian Fitzal. Comparing two objective methods for the aesthetic evaluation of breast cancer conservative treatment. *Breast Cancer Research and Treatment*, 116:149–152, 2009.
- [33] J. Lee, E. K. Beahm, M. A. Crosby, G. P. Reece, and M. K. Markey. Analysis of breast contour using rotated catenary. In *AMIA Annual Symposium Proceedings*, pages 432–436, 2010.
- [34] Min Soon Kim, Gregory P. Reece, Elisabeth K. Beahm, Michael J. Miller, E. Neely Atkinson, and Mia K. Markey. Objective assessment of aesthetic outcomes of breast cancer treatment: Measuring ptosis from clinical photographs. *Comput. Biol. Med.*, 37(1):49–59, 2007.
- [35] N. Isogai, K. Sai, H. Kammishi, M. Watatani, H. Inui, and H. Shiozaki. Quantitative analysis of the reconstructed breast using a 3-dimensional laser light scanner. *Ann Plast Surg*, 56(3):237 – 242, 2006.
- [36] L. Kovacs, M. Eder, R. Hollweck, A. Zimmermann, M. Settles, A. Schneider, M. Endlich, A. Mueller, K. Schwenzer-Zimmerer, N. A. Papadopoulos, and E. Biemer. Comparison between breast volume measurement using 3d surface imaging and classical techniques. *The Breast*, 16(2):137 – 145, 2007.
- [37] O. M. Tepper, J. G. Unger, K. H. Small, D. Feldman, N. Kumar, M. Choi, and N. S. Karp. Mammometrics: the standardization of aesthetic and reconstructive breast surgery. *Plast Reconstr Surg*, 125(1):393 – 400, 2010.
- [38] A. Losken, H. Seify, D. D. Denson, A. A. Paredes, and G. W. Carlson. Validating three-dimensional imaging of the breast. *Ann Plast Surg*, 54(5):471 – 476, 2005.

- [39] A. Losken, I. Fishman, D. D. Denson, H. R. Moyer, and G. W. Carlson. An objective evaluation of breast symmetry and shape differences using 3-dimensional images. *Ann Plast Surg*, 55(6):571 – 575, 2005.
- [40] H. R. Moyer, G. W. Carlson, T. M. Styblo, and A. Losken. Three-dimensional digital evaluation of breast symmetry after breast conservation therapy. *Journal of the American College of Surgeons*, 207(2):227 – 232, 2008.
- [41] G. Catanuto, P. Patete, A. Spano, A. Pennati, G. Baroni, and M. B. Nava. New technologies for the assessment of breast surgical outcomes. *Aesthetic Surgery Journal*, 29(6):505 – 508, 2009.
- [42] Paolo Patete, Marco Riboldi, Maria Spadea, Giuseppe Catanuto, Andrea Spano, Maurizio Nava, and Guido Baroni. Motion compensation in hand-held laser scanning for surface modeling in plastic and reconstructive surgery. *Annals of Biomedical Engineering*, 37:1877–1885, 2009.
- [43] Christoph Bert, Katherine G. Metheany, Karen Doppke, and George T. Y. Chen. A phantom evaluation of a stereo-vision surface imaging system for radiotherapy patient setup. *Medical Physics*, 32(9):2753–2762, 2005.
- [44] J. S. Cardoso and M. J. Cardoso. Breast contour detection for the aesthetic evaluation of breast cancer conservative treatment. In *5th International Conference on Computer Recognition Systems*, pages 518–525, 2007.
- [45] R. Sousa, J. S. Cardoso, J. F. Pinto da Costa, and M. J. Cardoso. Breast contour detection with shape priors. In *Proceedings of the 15<sup>th</sup> IEEE International Conference on Image Processing*, pages 1440–1443, 2008.
- [46] J. S. Cardoso, L. F. Teixeira, and M. J. Cardoso. Automatic breast contour detection in digital photographs. In *Proceedings of the International Conference on Health Informatics*, volume 2, pages 91–98, 2008.
- [47] H. P. Oliveira, A. Magalhaes, M. J. Cardoso, and J. S. Cardoso. An accurate and interpretable model for bcct.core. In *Proceedings of the 32<sup>nd</sup> Annual International Conference of the IEEE Engineering in Medicine and Biology Society*, pages 6158 – 6161, 2010.
- [48] Joao Miguel Trigo Soares. Uncalibrated stereo vision applied to breast cancer treatment aesthetic assessment. Master’s thesis, Faculdade de Engenharia da Universidade do Porto, 2011.
- [49] Shahram Izadi, David Kim, Otmar Hilliges, David Molyneaux, Richard Newcombe, Pushmeet Kohli, Jamie Shotton, Steve Hodges, Dustin Freeman, Andrew Davison, and Andrew Fitzgibbon. Kinectfusion: real-time 3d reconstruction and interaction using a moving depth camera. In *Proceedings of the 24th annual ACM symposium on User interface software and technology*, UIST ’11, pages 559–568, New York, NY, USA, 2011. ACM.
- [50] Papathanassiou C and Petrou M. Super-resolution: an overview. *IEEE International Geoscience and Remote Sensing Symposium (IGARSS05)*, 8:5655–5658, 2005.
- [51] Shmuel Peleg, Danny Keren, and Limor Schweitzer. Improving image resolution using sub-pixel motion. *Pattern Recogn. Lett.*, 5(3):223–226, March 1987.

- [52] Michal Irani and Shmuel Peleg. Improving resolution by image registration. *CVGIP: Graph. Models Image Process.*, 53(3):231–239, April 1991.
- [53] Sung C. Park, Min K. Park, and Moon G. Kang. Super-resolution image reconstruction: a technical overview. *IEEE Signal Processing Magazine*, 20(3):21–36, May 2003.
- [54] Sina Farsiu, Dirk Robinson, Michael Elad, and Peyman Milanfar. Fast and robust multi-frame super-resolution. *IEEE Transactions on Image Processing*, 19(11):1327–1344, 2010.
- [55] Weisheng Dong, Lei Zhang, Guangming Shi, and Xiaolin Wu. Image deblurring and super-resolution by adaptive sparse domain selection and adaptive regularization. *IEEE Transactions on Image Processing*, 20(7):1838–1857, 2011.
- [56] Xuelong Li, Yanting Hu, Xinbo Gao, Dacheng Tao, and Beijia Ning. A multi-frame image super-resolution method. *Signal Process.*, 90(2):405–414, February 2010.
- [57] Patrick Vandewalle, Sabine Süsstrunk, and Martin Vetterli. A frequency domain approach to registration of aliased images with application to super-resolution. *EURASIP Journal on Applied Signal Processing*, 2006:1–14, March 2006.
- [58] Jianchao Yang, John Wright, Thomas Huang, and Yi Ma. Image super-resolution via sparse representation. *IEEE Transactions on Image Processing*, 13, 2003.
- [59] L. C. Pickup. *Machine Learning in Multi-frame Image Super-resolution*. PhD thesis, University of Oxford, February 2008.
- [60] V. Cheung, B. J. Frey, and N. Jojic. Video Epitomes. In *CVPR*, volume 1, pages 42–49, 2005.
- [61] Patrick Vandewalle. *Super-Resolution from Unregistered Aliased Images*. PhD thesis, Ecole Polytechnique Federale de Lausanne, 2006.
- [62] Weisheng Dong, Lei Zhang, Guangming Shi, and Xiaolin Wu. Nonlocal back-projection for adaptive image enlargement. In *ICIP*, pages 349–352, 2009.
- [63] D Keren, S Peleg, and R Brada. Image sequence enhancement using sub-pixel displacements, 1988.
- [64] B. Marcel, M. Briot, and R. Murrieta-Cid. Calcul de translation et rotation par la transformation de fourier. *Journal Traitement du Signal*, 14(2):135–149, 1997.
- [65] Luca Lucchese and Guido Maria Cortelazzo. A noise-robust frequency domain technique for estimating planar roto-translations. *IEEE Transactions on Signal Processing*, 48(6):1769–1786, 2000.
- [66] Maximilian Eder, Fee V Waldenfels, Alexandra Swobodnik, Markus Kloppel, Ann-Kathrin Pape, Tibor Schuster, Stefan Raith, Elena Kitzler, Nikolaos A Papadopoulos, Hans-Gunther Machens, and et al. Objective breast symmetry evaluation using 3-d surface imaging. *Breast Edinburgh Scotland*, pages 1–7, 2011.
- [67] Daniel Herrera C, Juho Kannala, and Janne Heikkila. Joint depth and color camera calibration with distortion correction. *IEEE Transactions on Pattern Analysis and Machine Intelligence*, 99, 2012.